Enumeration and investigation of acute 0/1-simplices modulo the action of the hyperoctahedral group

Brandts, J.; Cihangir, A.

DOI
10.1515/spma-2017-0014

Publication date
2017

Document Version
Final published version

Published in
Special Matrices

Research Article **Open Access**

Jan Brandts* and Apo Cihangir

Enumeration and investigation of acute 0/1-simplices modulo the action of the hyperoctahedral group

https://doi.org/10.1515/spma-2017-0014
Received April 12, 2017; accepted August 21, 2017

Abstract: The convex hull of $n+1$ affinely independent vertices of the unit n-cube I^n is called a 0/1-*simplex*. It is *nonobtuse* if none its dihedral angles is obtuse, and *acute* if additionally none of them is right. In terms of linear algebra, acute 0/1-simplices in I^n can be described by nonsingular 0/1-matrices P of size $n \times n$ whose Gramians $G = P^\top P$ have an inverse that is strictly diagonally dominant, with negative off-diagonal entries [6, 7].

The first part of this paper deals with giving a detailed description of how to efficiently compute, by means of a computer program, a representative from each orbit of an acute 0/1-simplex under the action of the *hyperoctahedral group* $\mathcal{B}_n$ [17] of symmetries of I^n. A side product of the investigations is a simple code that computes the *cycle index* of $\mathcal{B}_n$, which can in explicit form only be found in the literature [11] for $n \le 6$. Using the computed cycle indices for $\mathcal{B}_3, \ldots, \mathcal{B}_{11}$ in combination with Pólya's theory of enumeration shows that acute 0/1-simplices are extremely rare among all 0/1-simplices.

In the second part of the paper, we study the 0/1-matrices that represent the acute 0/1-simplices that were generated by our code from a mathematical perspective. One of the patterns observed in the data involves *unreduced upper Hessenberg* 0/1-matrices of size $n \times n$, block-partitioned according to certain *integer compositions* of n. These patterns will be fully explained using a so-called *One Neighbor Theorem* [4]. Additionally, we are able to prove that the volumes of the corresponding acute simplices are in one-to-one correspondence with the part of *Kepler's Tree of Fractions* [1, 24] that enumerates $\mathbb{Q} \cap (0, 1)$. Another key ingredient in the proofs is the fact that the Gramians of the unreduced upper Hessenberg matrices involved are *strictly ultrametric* [14, 26] matrices.

Keywords: Acute simplex; 0/1-matrix; Hadamard conjecture; hyperoctahedral group; cycle index; Pólya enumeration theorem; Kepler's tree of fractions; strictly ultrametric matrix

MSC: 05A99

1 Introduction

A 0/1-simplex is an n-dimensional 0/1-polytope [23] with $n+1$ vertices. Equivalently, it is the convex hull of $n+1$ of the 2^n elements of the set $\mathbb{B}^n$ of vertices of the unit n-cube I^n whenever this hull has dimension n. To support the mathematical studies of 0/1-simplices, and in particular of those whose dihedral angles are all *nonobtuse* or even *acute* [7], we investigate how to enumerate such 0/1-simplices modulo the action of the hyperoctahedral group $\mathcal{B}_n$ of symmetries of I^n by means of a computer program. The motivation to generate

***Corresponding Author: Jan Brandts:** Korteweg-de Vries Institute for Mathematics, University of Amsterdam, P.O. Box 94248, 1090 GE Amsterdam, Netherlands, E-mail: J.H.Brandts@uva.nl
Apo Cihangir: Korteweg-de Vries Institute for Mathematics, University of Amsterdam, P.O. Box 94248, 1090 GE Amsterdam, Netherlands

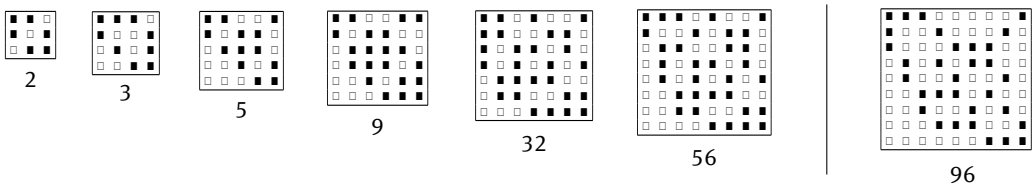

Figure 1: 0/1-matrices with maximal determinant that represent *acute* 0/1-simplices.

such computational data was quite appropriately phrased by Günther Ziegler in Chapter 1 of *Lectures on* 0/1-*Polytopes* [23], as "*Low-dimensional intuition does not work!*".

This statement expresses the fact that although it is tempting to formulate conjectures on n-dimensional 0/1-polytopes and related 0/1-matrices based on computational data obtained for a few small values of n, these conjectures often fail to be true. Finding out that a conjecture is false using general mathematical arguments may be much harder than generating the necessary computational data for large enough n to *disprove* it, not in the least because the tendency towards a conjecture is rather to believe its validity and aim to prove it. This is why we concentrate on the enumeration problem for acute 0/1-simplices. Using the date produced by the enumeration, we will also formulate and prove some mathematical results on certain classes of 0/1-matrices. We will summarize the most important of these results in Section 1.2. First, in Section 1.1, we give two examples that illustrate Ziegler's claim above, also based on the computational data.

Remark 1.1. Especially the larger 0/1-matrices in this paper we will often display as a picture of an array with black and white squares representing its ones and zeros, respectively.

1.1 Two examples in which low dimensional intuition does not work

A first example of a statement that is valid in I^n for $n \leq 8$ but that does not hold in I^9 is the following. In Figure 1 we display 0/1-matrices P having maximal absolute value of the determinant, when ranging over all those $n \times n$ matrices whose n columns together with the origin are the vertices of a so-called *acute* 0/1-simplex. See Definition 5.1 for a linear algebraic characterization acute 0/1-simplices and the 0/1-matrices associated with them. For $n \leq 8$, these values turn out to be even maximal when ranging over *all* 0/1-matrices of size $n \times n$. However, the maximum over all 0/1-matrices of size 9×9 is 144 and not 96.

This, of course, disproves the conjecture that maximal determinants of 0/1-matrices are attained by 0/1-matrices that represent acute 0/1-simplices. Notwithstanding, the Hadamard maximal determinant conjecture [19] is equivalent [18] with the existence of a *regular* simplex in I^n for dimensions n whose remainder after devision by 4 equals 3. Regular simplices have acute dihedral angles, and indeed, the 3×3 and the 7×7 matrix in Figure 1 are so-called *Hadamard matrices*. This motivates a further study of acute 0/1-simplices and their determinants, as the set of acute 0/1-simplices is a small and highly structured set in which the Hadamard matrices figure as the most structured ones. It thus puts the Hadamard matrices in a wider context in which, as far as we know, they have not yet been studied.

As a second example in which low dimensional intuition does not work, here is a statement that holds in I^n for all $n \leq 7$: the Gramian $G = P^\top P$ of any 0/1-matrix P whose columns together with the origin are the vertices of an acute simplex is a *strictly ultrametric* matrix [14, 26]. A strictly ultrametric matrix is a highly structured *positive* matrix in the sense that all its 3×3 principal submatrices are, modulo simultaneous permutation of rows and columns, of the form

$$\begin{bmatrix} d & b & a \\ b & c & a \\ a & a & f \end{bmatrix}, \quad \text{with} \quad a \leq b < c \leq d \quad \text{and} \quad a < f. \tag{1}$$

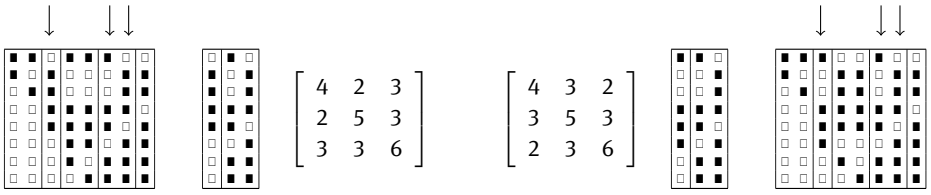

Figure 2: Examples of 0/1-matrices representing acute 0/1-simplices whose Gramians are *not* ultrametric. Columns 3,6,7 do not satisfy the inequalities in (68).

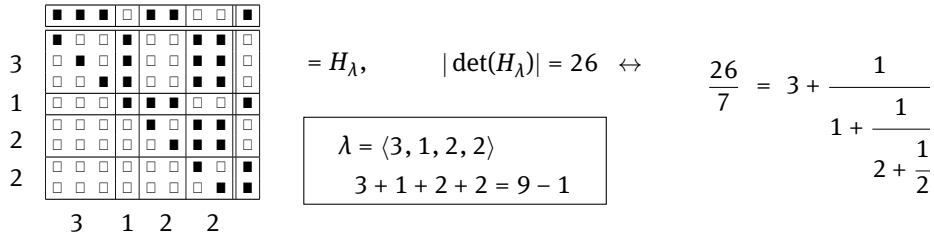

Figure 3: The matrix H_λ for a composition $\lambda = \langle \lambda_1, \ldots, \lambda_k \rangle$ of $n-1$ with first and last parts larger than one, and its determinant as numerator of the continued fraction $[\lambda_1; \lambda_2, \ldots, \lambda_k]$.

Even though the columns of the two 8×8 matrices displayed in Figure 2 together with the origin are indeed vertices of acute 0/1-simplices in I^8, their Gramians are however *not* strictly ultrametric. In both matrices, the inner products between columns 3, 7, and 8 do not satisfy the relations in (1), not even after simultaneous row- and column permutations. We will return to strictly ultrametric and related matrices in Section 6, because they will turn out to be a powerful tool to prove our main results. See also [3] for a detailed account on the geometric properties of the special type of simplices whose Gramians are ultrametric.

1.2 Main results obtained from analyzing the generated data

A positive result in this context is as follows. Let $n \geq 3$, and let the ordered tupel $\lambda = \langle \lambda_1, \ldots, \lambda_k \rangle$ be a *composition* of the integer $n-1$ whose first and last part are at least 2. Associate with λ the $n \times n$ matrix H_λ as is done for the example $\lambda = \langle 3, 1, 2, 2\rangle$ in Figure 3. The matrix H_λ is constructed as an *unreduced upper Hessenberg* matrix with identity matrices I_j of size $\lambda_j \times \lambda_j$ covering the lower co-diagonal from top left to bottom right. The matrices $I_1, \ldots, I_k$ define a *checkerboard pattern* in H_λ above $I_1, \ldots, I_k$, with blocks containing either only ones, or only zero entries, where the blocks directly bordering I_j and I_{j+1} contain only ones. This uniquely defines H_λ in terms of the composition λ.

In Section 6.2 we will prove the following results in this context.

Theorem 1.2. *Let H be an $n \times n$ unreduced upper Hessenberg 0/1-matrix whose columns and the origin are the $n+1$ vertices of a simplex $S \subset I^n$ with acute dihedral angles only. Then, possibly after exchanging its first two rows and/or last two columns, H is equal to the matrix H_λ for some composition $\lambda = \langle \lambda_1, \ldots, \lambda_k \rangle$ of $n-1$ with first and last parts larger than one. Moreover,*

$$|\det(H_\lambda)| = f_k, \quad \text{where} \quad \frac{f_k}{g_k} = \lambda_1 + \cfrac{1}{\lambda_2 + \cfrac{1}{\ddots + \cfrac{1}{\lambda_k}}}, \quad \gcd(f_k, g_k) = 1. \tag{2}$$

Conversely, each such matrix H_λ has the property that its Gramian is strictly ultrametric, which implies that its columns together with the origin are the vertices of an acute 0/1-simplex.

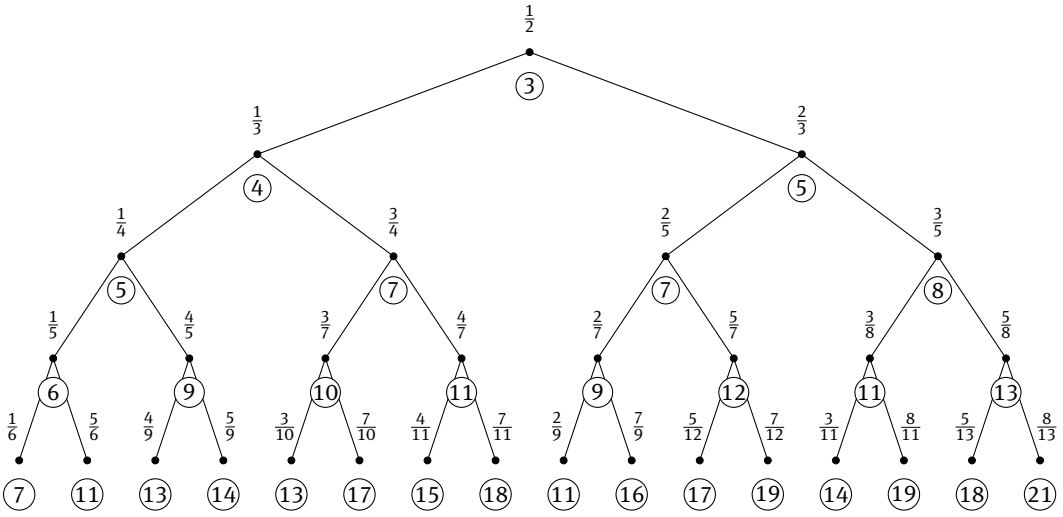

Figure 4: Part of Kepler's *Tree of Fractions* and absolute determinants of the matrices H_λ.

As a corollary of this theorem, all attainable absolute values of the determinant function on the set of all unreduced $n \times n$ upper Hessenberg 0/1-matrices H for which $(H^\top H)^{-1}$ is a diagonally dominant Stieltjes matrix with negative off-diagonal entries, can be explicitly read from a part of *Kepler's Tree of Fractions* [24]. This part is depicted in Figure 4. It has the fraction $\frac{1}{2}$ as root. The children of a vertex $\frac{p}{q}$ are $\frac{p}{p+q}$ and $\frac{q}{p+q}$. Transversing the tree level by level corresponds to an enumeration of all the rationals $\mathbb{Q} \cap (0, 1)$. The circled integers displayed in Figure 4 below each vertex equal the sum of numerator and denominator of the fraction belonging to that vertex. At level k these integers correspond to the absolute values of the determinants of each of the 2^k matrices H_λ of size $(k + 4) \times (k + 4)$.

Observe that the determinants in the rightmost branch in the tree equal the Fibonacci numbers, which were proved in [12] to be the maximal value of the determinant function over *all* $n \times n$ Hessenberg 0/1-matrices. We can now conclude that this maximum is (also) attained by matrices representing *acute* simplices. More generally we see that any branch of the tree that, starting at a given vertex p/q corresponding to the determinantal value $p + q$, extends only to the right, yields a Fibonacci-type sequence $d_r(j)$,

$$d_r(j + 2) = d_r(j) + d_r(j + 1) \quad \text{with} \quad d_r(-1) = p, \quad d_r(0) = q \quad \text{and} \quad d_r(1) = p + q, \tag{3}$$

whereas any branch from a vertex p/q that extends only to the left, yields a family of acute 0/1-simplices with determinants increasing linearly as

$$d_\ell(j) = jp + q. \tag{4}$$

The corresponding matrices H_λ in this latter case have integer compositions of which the last part increases by one when the size of H_λ increases by one while all the other parts of λ remain the same. The existence of such families with linearly increasing determinants was first observed in [5]. In Section 6 we give a full explanation of their structure.

1.3 Outline of the paper

Our aim is to give a self-contained account of all necessary ingredients. For this, we first recall in Section 2 the group structure of $\mathcal{B}_n$ and the permutation subgroup of S_{2^n} it induces on the set $\mathbb{B}^n$ of 0/1-vectors of length n. These induced permutations were studied by Harrison and High, who derived a formula in [20] for the corresponding *cycle index polynomial* Z_n of $\mathcal{B}_n$. This formula was later claimed to be simplified by Chen in [10], who also studied the induced permutations of the *edges* of I^n. Unfortunately, in view of the standard counting paradigm of Pólya [27], neither formula allows a straightforward evaluation, modulo the induced

Table 1: The number $a(n)$ of *acute* $0/1$ n-simplices in I^n related to their *total* number $s(n)$. All cardinalities are modulo the action of $\mathcal{B}_n$.

n	1	2	3	4	5	6	7	8	9	10	11
$a(n)$	1	0	1	1	2	6	13	29	67	162	392
$s(n)$	1	1	6	27	472	19735	2773763	1245930065	$1.8e12$	$8.7e15$	$1.3e20$

action of $\mathcal{B}_n$ on $\mathbb{B}^n$, of the number ε_n^k of $0/1$-polytopes in I^n with k vertices. Therefore, here we will aim for a more pragmatic approach, also motivated by the fact that for $n > 6$ we failed to find explicit expressions for Z_n in the literature. First, in Section 2, we give transparent algorithmic descriptions of how to compute Z_n by means of a simple computer code. This code yields Z_n as a table of coefficients and exponents of monomials in a minimal effort: the table for $n = 9$ in Section A was, for instance, produced on a simple laptop within half a second. As a next step, in Section 3 we explain how to compute, modulo the action of $\mathcal{B}_n$, the numbers ε_n^k of $0/1$-polytopes with k vertices by applying Pólya's theory to the specific situation at hand. Again, the emphasis is to show how to algorithmically obtain the *concrete values* of ε_n^k by means of a computer code, using the tables for the cycle indices of $\mathcal{B}_n$. As we will be interested in $0/1$-simplices, we pay special attention to the values $k \le n + 1$. In Section A we present a selection of the numbers produced by the algorithms.

In Section 4 we change our perspective from $0/1$-polytopes and two-colorings to $0/1$-*matrices*. A $0/1$-polytope c with k vertices can trivially be represented by a $0/1$ matrix of size $n \times k$ whose columns are the vertices of c. Although convenient, this unfortunately introduces another non-trivial redundancy, as there are $k!$ matrices having this property. Consequently, we investigate how to establish whether two given $0/1$-matrices represent $0/1$-polytopes in the same orbit under $\mathcal{B}_n$. From all $0/1$-matrices representing all the $0/1$-polytopes in the same orbit under $\mathcal{B}_n$, we select one designated matrix, the *minimal matrix representation* $P^\star$, and study its properties. As a first application, this concept enables us to enumerate all $0/1$-triangles in I^n modulo the action of $\mathcal{B}_n$: we give the minimal matrix representation of each of the ε_n^2 distinct orbits of $0/1$-triangles under $\mathcal{B}_n$ using $\mathcal{O}(1)$ arithmetic operations per triangle. We do the same for the subset of *acute* $0/1$-triangles. Basically, we parametrize both sets with the points with integer coordinates in a three-dimensional polyhedron, which in both cases turns out to be a simple tetrahedron. We also derive an explicit formula for their cardinalities by counting the integer points in the respective tetrahedra. In theory, the same can be done for k-simplices. This however results in enumerating and counting the points with integer coordinates in a polytope of dimension $2^k - 1$ constrained by at most $(k + 1)!$ inequalities. Although the enumeration would still cost $\mathcal{O}(1)$ per k-simplex independent of n, the dependence on k makes such enumeration impractical.

As a consequence of this intractability, in Section 5 we use the assistance of the computer to extend the minimal matrix representations of the acute $0/1$-*triangles* from Section 4 into minimal matrix representations of acute $0/1$-*tetrahedra*, and similarly further into minimal matrix representations of all acute $0/1$-*simplices* with $n + 1$ vertices. Since acute simplices have acute *facets* [16], each minimal matrix representation of an acute $0/1$-tetrahedron equals a minimal matrix representation T of an acute $0/1$-triangle *with one additional column* t *appended*. Hence, in theory, one could append one by one all feasible columns t to T such that $[T|t]$ represents an acute tetrahedron, discard the ones that do not yield a minimal matrix representation, and continue to add more columns. Unfortunately, the verification of *minimality* is computationally much more expensive than verifying *acuteness*. It may thus be much quicker to find out if $[T|t]$ can be extended to the desired number of columns, then to find out if it is minimal. This saves computational effort if it *cannot* be acutely extended. According to the data from Table 1 (see also Section A), acute n-simplices in I^n are extremely rare. Thus it seems likely that simply extending a minimal matrix representation until no acute extensions are available anymore is quicker than discarding the matrix representations that are not minimal. However, it turns out that the amount of data in the intermediate phases becomes unacceptably large. Thus, the challenge to make our algorithms as efficiently as possible is therefore nontrivial, and involves the well-known struggle between time and memory requirements. It requires a subtle balance between spending time

in computing minimal matrix representations, and allowing the data to take more and more memory space. Along the way, and also for the purpose of mathematical analysis, we introduce the sets of *candidate acute extensions* $\mathcal{C}^n(S)$ and of *acute extensions* $\mathcal{A}^n(S)$ of a given acute simplex $S \subset I^n$. Using the theory of symmetric inverse M-matrices (also called Stieltjes matrices) [21, 22], it is possible to derive relations between the members of these sets that make their computation in many cases much less expensive than at first sight. In Section A.3 we display the minimal matrix representations of all the acute 0/1-simplices in I^n for $n \in \{3, 4, \ldots, 9\}$.

In Section 6 we analyze these minimal matrix representations. Proofs of the results given in Section 1.2 will be based on the so-called *One Neighbor Theorem* for acute 0/1-simplices [4]. This theorem states that the set $\mathcal{C}^n(S)$ of candidate acute extentions of a simplex $S \subset I^n$ with n vertices consists of at most two antipodal points. As a consequence, only points in higher dimensional cubes that project orthogonally on this antipodal pair can be added to form acute 0/1-simplices with more vertices. If one demands their matrix representation to be unreduced upper Hessenberg, this limits the possible options even further. What results is a complete description of the corresponding simplices in Section 6.2 together with the values of the determinants of their matrix representations in terms of continued fractions. Apart from the One Neighbor Theorem, we also use the properties of *strictly ultrametric matrices* [26] to prove acuteness of the simplices involved.

2 The hyperoctahedral group $\mathcal{B}_n$ and its induced permutations

Write $I^n = [0, 1]^n$ for the unit n-cube and $\mathbb{B}^n = \{0, 1\}^n$ for the set of its vertices. Let $\mathcal{B}_n$ be the set of all rigid transformations $h : I^n \to I^n$. Endowing $\mathcal{B}_n$ with the usual composition of map as multiplication rule, it becomes the *hyperoctahedral group* of n-cube symmetries, with the *dihedral* group $\mathcal{B}_2$ and the *octahedral* group $\mathcal{B}_3$ as well-known instances. Each $h \in \mathcal{B}_n$ bijectively maps k-facets of I^n to k-facets and thus induces a permutation of these k-facets; in particular, it permutes $\mathbb{B}^n$. To describe this latter permutation, we choose the following bijection β as *numbering* of $\mathbb{B}^n$. It interprets the 0/1-vector $v \in \mathbb{B}^n$ as a binary number. Each $h \in \mathcal{B}_n$ induces a permutation $\pi_h \in S_{2^n}$ of the numbers $0, \ldots, 2^n - 1$ via β by

$$\pi_h : \quad \{0, \ldots, 2^n - 1\} \to \{0, \ldots, 2^n - 1\} : \quad k \mapsto (\beta \circ h \circ \beta^{-1})(k). \tag{5}$$

In Section 3 we will count the number of 0/1-*polytopes* modulo n-cube symmetries using Pólya's Theorem [27]. For this we need to know *how many* permutations π_h *of which cycle type* are induced in S_{2^n} when h ranges over $\mathcal{B}_n$. Recalling that any permutation π of ℓ objects can be written as the product of *disjoint cycles*, we can define the *cycle type* of π.

Definition 2.1 (Cycle type)**.** If $\pi \in S_\ell$ has t_i cycles of length i in its cycle factorization, then the vector

$$t(\pi) = (t_1, \ldots, t_\ell), \quad \text{with} \quad t_1 \cdot 1 + \cdots + t_\ell \cdot \ell = \ell \tag{6}$$

is an integer partition of ℓ called the *cycle type* of π.

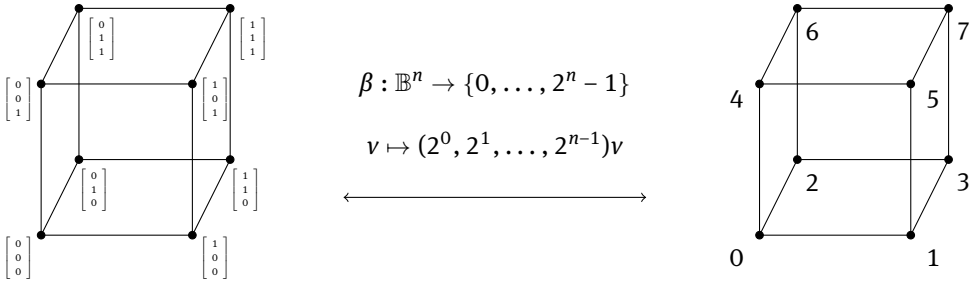

Figure 5: Binary-to-decimal numbering β of the vertex set $\mathbb{B}^n$ of I^n, depicted for $n = 3$.

From basic algebra we know that the cycle types of two permutations in S_ℓ coincide if and only if they are *conjugate*.

Lemma 2.2. *Let $\pi, \tilde{\pi} \in S_\ell$, then $t(\tilde{\pi}) = t(\pi)$ if and only if $\tilde{\pi} = \sigma^{-1} \circ \pi \circ \sigma$ for some $\sigma \in S_\ell$.*

An important consequence is the following corollary, whose formulation uses (5).

Corollary 2.3. *If two elements $h, \tilde{h}$ are conjugate in $\mathcal{B}_n$ then $t(\pi_h) = t(\pi_{\tilde{h}})$ in S_{2^n}.*

Proof. The mapping $\mathcal{B}_n \to S_{2^n} : f \mapsto \pi_f$ is an injective homomorphism. Therefore, if $\tilde{h} = g \circ h \circ g^{-1}$ then $\pi_{\tilde{h}} = \pi_g \circ \pi_h \circ \pi_g^{-1}$. Lemma 2.2 now proves the statement. □

Remark 2.4. The table in (3) constitutes an example of the fact that $t(\pi_g) = t(\pi_h)$ while g and h are not conjugate in $\mathcal{B}_n$, hence the converse implication in Corollary 2.3 does not hold.

Corollary 2.3 shows that counting how many permutations of which type are induced by the elements of $\mathcal{B}_n$ reduces to the following two tasks,

- find the cycle type of π_h of a single element h from each conjugacy class of $\mathcal{B}_n$,
- count the number of elements in each conjugacy class of $\mathcal{B}_n$.

Before performing these tasks in Section 2.3, we recall some basic facts about $\mathcal{B}_n$. We identify two subgroups $\mathcal{B}_n^c$ and $\mathcal{B}_n^p$ of $\mathcal{B}_n$ and show that $\mathcal{B}_n = \mathcal{B}_n^p \times \mathcal{B}_n^c$. This enables us to associate with each $h \in \mathcal{B}_n$ a so-called *signed permutation*. The corresponding *signed cycle type* of such a signed permutation will then be used to describe and count the conjugacy classes of $\mathcal{B}_n$, and consequently, the number and cycle type of their induced permutations in S_{2^n}.

2.1 The subgroups $\mathcal{B}_n^c$ and $\mathcal{B}_n^p$: complementations and permutations

Let the n-tupel $\langle e_1, \ldots, e_n \rangle$ be the standard basis for $\mathbb{R}^n$. For $j \in \{1, \ldots, n\}$, let $c_j : I^n \to I^n : x \mapsto e_j + x - 2e_j e_j^\top x$ be the reflection in the affine hyperplane $2x_j = 1$. The set $\{c_1, \ldots, c_n\}$ generates a subgroup $\mathcal{B}_n^c$ of $\mathcal{B}_n$. Note that $c_i \circ c_j = c_j \circ c_i$ and $c_j^2 = id$. Thus, the mapping

$$\mathbb{B}^n \to \mathcal{B}_n^c : \quad w \mapsto c_w = c_1^{w_1} \circ c_2^{w_2} \circ \cdots \circ c_n^{w_n} \tag{7}$$

is a bijection, showing that $|\mathcal{B}_n^c| = 2^n$. One can verify that $c_w(v) = \mathrm{xor}(w, v) = (w + v) \bmod 2$, where xor is the logical *exclusive or* operation performed entry-wise on the pair $w, v \in \mathbb{B}^n$.

Next, for each $j \in \{2, \ldots, n\}$, consider the reflection $s_j : I^n \to I^n : x \mapsto x - (e_1 - e_j)(e_1 - e_j)^\top x$ in the hyperplane $x_1 = x_j$. The set $\{s_2, \ldots, s_n\}$ generates a subgroup $\mathcal{B}_n^p$ of $\mathcal{B}_n$. The action of s_j on $v \in \mathbb{B}^n$ interchanges the first and jth entry of v. Since *each* permutation of n objects is a product of transpositions with the first object [15], we conclude that $|\mathcal{B}_n^p| = n!$.

For each permutation $u = [u(1), \ldots, u(n)] \in S_n$, we write p_u for the element from $\mathcal{B}_n^p$ defined by its action on $\mathbb{B}^n$ as

$$(p_u)(v) = v \circ u = (v_{u(1)}, \ldots, v_{u(n)})^\top. \tag{8}$$

Definition 2.5 (Coordinate complementation and permutation)**.** An element $c_w \in \mathcal{B}_n^c$ will be called a *coordinate complementation* and an element $p_u \in \mathcal{B}_n^p$ a *coordinate permutation*.

Example. Consider the group $\mathcal{B}_3$ of unit cube symmetries. It contains a subgroup $\mathcal{B}_3^c$ of order $8 = 2^3$ with generators c_1, c_2, c_3, the reflections in the planes $2x_j = 1$, and a subgroup of order $6 = 3!$ with generators s_2 and s_3, the reflectors in the planes $x_1 = x_2$ and $x_1 = x_3$. To illustrate the actions of elements from $\mathcal{B}_3^c$

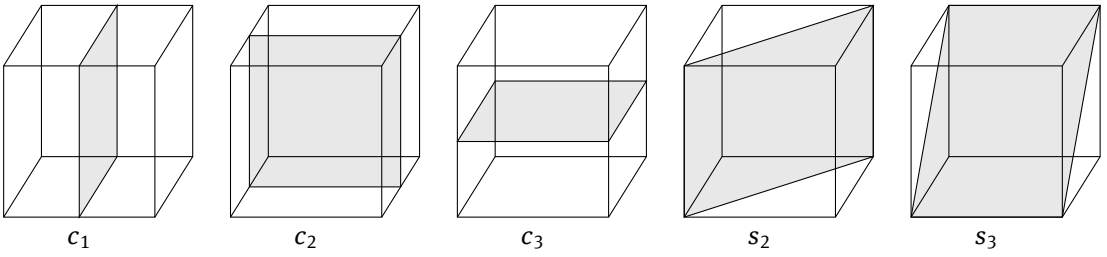

Figure 6: Generators of $\mathcal{B}_3$: complementations c_1, c_2, c_3 and the permutations s_2 and s_3.

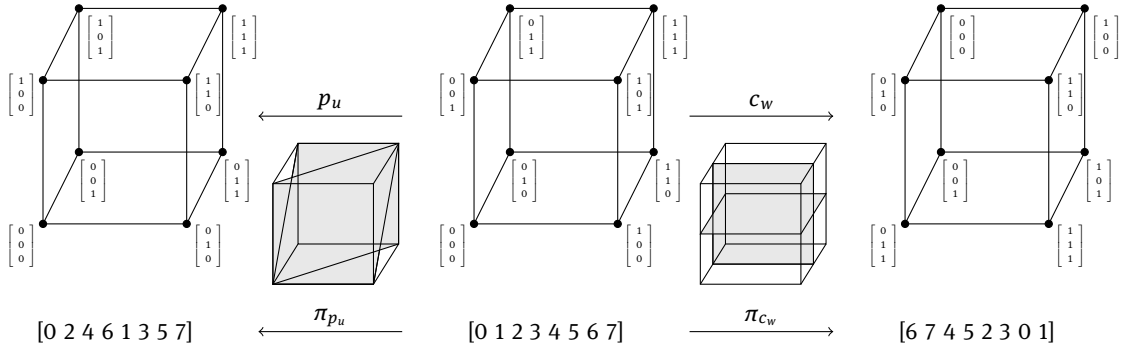

Figure 7: A complementation c_w, a permutation p_u, and their induced permutations in S_8.

and $\mathcal{B}_3^p$, let for instance $w = (0,1,1)^\top$. Then $c_w \in \mathcal{B}_n^c$ acts on I^3 as depicted in the right part of Figure 7. Note that $c_w = c_1 \circ c_2 = c_2 \circ c_1$. Also given is its induced permutation $\pi_{c_w} \in S_8$. Next, given the permutation $u = [3\ 1\ 2] \in S_3$, the action of $p_u \in \mathcal{B}_n^p$ on I^3 is depicted on the left, also together with its induced permutation $\pi_{p_u} \in S_8$. Observe that $p_u = s_3 \circ s_2$, but that the product $s_3 \circ s_2$ does not equal p_u.

2.2 $\mathcal{B}_n$ and the group of signed permutations of n objects

An n-cube symmetry $h \in \mathcal{B}_n$ is a rigid transformation and thus an affine isometry. As such, it is uniquely determined by the combination of both the items (1) and (2), being

(1) the vertex $v \in \mathbb{B}^n$ that is mapped to the origin by h,

(2) how the n vertices of I^n at distance one from v are mapped to $e_1, \ldots, e_n$.

Note that c_v is the unique element from $\mathcal{B}_n^c$ with $c_v(v) = 0$. Also note that $p_u(0) = 0$ and $p(e) = e$ for all $p_u \in \mathcal{B}_n^p$, where $e = e_1 + \cdots + e_n$ is the *all-ones vector*. Thus, we have that

$$\left\{h \in \mathcal{B}_n \quad | \quad h(v) = 0\right\} \quad = \quad \left\{h = p_u \circ c_v \quad | \quad p_u \in \mathcal{B}_n^p\right\}. \tag{9}$$

Also observe that each $p_u \in \mathcal{B}_n^p$ corresponds to a unique permutation of the basis vectors.

Corollary 2.6. *For each $h \in \mathcal{B}_n$ there exist unique pair $p_u \in \mathcal{B}_n^p$ and $c_v \in \mathcal{B}_n^c$ such that*

$$p_u \circ c_v = h = c_{p_u(v)} \circ p_u. \tag{10}$$

One of the consequences of the uniqueness is that the order $|\mathcal{B}_n|$ of $\mathcal{B}_n$ equals $n!2^n$. Another consequence is that we can now identify with each $h \in \mathcal{B}_n$ a so-called *signed permutation*.

Definition 2.7 (Signed permutation)**.** *We will index $h \in \mathcal{B}_n$ as h_w, where the vector w, called a* signed permutation*, has entries given by*

$$w_j = u_j \quad \text{if } v_j = 0 \quad \text{and} \quad w_j = \overline{u_j} \quad \text{if } v_j = 1, \tag{11}$$

where u and v are the indexes of the unique $p_u \in \mathcal{B}_n^p$ and $c_v \in \mathcal{B}_n^c$ such that $h = p_u \circ c_v$.

The set of all signed permutations of n objects is obviously isomorphic to $\mathcal{B}_n$.

2.3 Conjugacy classes and signed cycle types in $\mathcal{B}_n$

We now introduce the *signed cycle type* of a signed permutation. It will have the property that two elements in $\mathcal{B}_n$ are conjugate if and only if they have the same signed cycle type.

Definition 2.8 (Signed cycle type)**.** *Let $h = p_u \circ c_v$ with $p_u \in \mathcal{B}_n^p$ and $c_v \in \mathcal{B}_n^c$. For each cycle γ in the decomposition of the permutation u into disjoint cycles, set*

$$\chi(\gamma) = \sum_{j\in\gamma} v_j. \tag{12}$$

Let u_+ be the product of the cycles γ of u for which $\chi(\gamma)$ is even, and u_- such that $u = u_+ \circ u_-$. Then the $2 \times n$ array

$$t_\pm(h) = \begin{cases} t(u_+) \\ t(u_-) \end{cases} \tag{13}$$

where t is the cycle type from Definition 2.1, is called the signed cycle type *of h.*

Note that the signed cycle types of the elements $h \in \mathcal{B}_n$ are in one-to-one correspondence with the *double partitions* [17] of n, which are ordered pairs of partitions of k and ℓ with $k + \ell = n$.

Example. Let $h_w \in \mathcal{B}_{10}$ be the ten-cube symmetry indexed by the *signed permutation*

$$w = [2\ \overline{6}\ 7\ \overline{4}\ 8\ \overline{1}\ 9\ 5\ \overline{10}\ 3]. \tag{14}$$

Then $h_w = p_u \circ c_v$, with $v = (0, 1, 0, 1, 0, 1, 0, 0, 1, 0)^\top$ and $u = [2\ 6\ 7\ 4\ 8\ 1\ 9\ 5\ 10\ 3]$. The latter can be written as a product of cycles as $u = (1\ 2\ 6)(3\ 7\ 9\ 10)(4)(5\ 8)$. This results in $\chi(1\ 2\ 6) = v_1 + v_2 + v_6 = 2$ and similarly, $\chi(5\ 8) = 0$, and $\chi(3\ 7\ 9\ 10) = \chi(4) = 1$. Therefore, $u_+ = (1\ 2\ 6)(5\ 8)$ and $u_- = (3\ 7\ 9\ 10)(4)$ and thus,

$$t_\pm(h) = \begin{cases} (0, 1, 1, 0, 0, 0, 0, 0, 0, 0) \\ (1, 0, 0, 1, 0, 0, 0, 0, 0, 0) \end{cases}, \tag{15}$$

is the *signed cycle type* of h, corresponding to the partitions $2 + 3$ and $1 + 4$ of 5. ◊

In view of Corolary 2.3, we will now state one of the main results in this section.

Theorem 2.9. *Two elements $g, h \in \mathcal{B}_n$ are conjugate in $\mathcal{B}_n$ if and only $t_\pm(g) = t_\pm(h)$.*

Thus, we have been successful in our aim to characterize the conjugacy classes of $\mathcal{B}_n$. Now we will consider the question of counting the number of elements of each of these classes. Firstly, Definition 2.1 implies that S_ℓ has $p(\ell)$ conjugacy classes, where $p(\ell)$ stands for the number of integer partitions of ℓ. The sizes of these classes are well known.

Proposition 2.10. *The size of each conjugacy class of S_ℓ, being the number of $\sigma \in S_\ell$ such that $t(\sigma) = (t_1, \ldots, t_\ell)$ for a given cycle type $(t_1, \ldots, t_\ell)$ equals*

$$\left[\begin{array}{c} \ell \\ t \end{array}\right] = \frac{\ell!}{1^{t_1} \cdot \ldots \cdot \ell^{t_\ell} \cdot t_1! \cdot \ldots \cdot t_\ell!}. \tag{16}$$

Similarly, writing $\Delta(n)$ for the number of double partitions of n, we have that $\Delta(n)$ is the number of conjugacy classes of $\mathcal{B}_n$ and that

$$\Delta(n) = \sum_{k=0}^{n} p(k)p(n-k). \tag{17}$$

Table 2: Sequences A000041 and A000712 in the *Online Encyclopedia of Integer Sequences*.

n	0	1	2	3	4	5	6	7	8	9	10	11	12	13
$p(n)$	1	1	2	3	5	7	11	15	22	30	42	56	77	101
$\Delta(n)$	1	2	5	10	20	36	65	110	185	300	481	752	1165	1770

For illustration, we list here the first few values of p and Δ in Table 2.

Proposition 2.11. *The number of elements in $\mathcal{B}_n$ of the signed cycle type*

$$t_{\pm}(h) = \left\{ \begin{array}{c} (t_1, \ldots, t_n) \\ (s_1, \ldots, s_n) \end{array} \right. \quad \text{equals} \quad \binom{n}{k} \left[\begin{array}{c} k \\ t \end{array} \right] \left[\begin{array}{c} \ell \\ s \end{array} \right] 2^{n-\sum(t_j+s_j)} \tag{18}$$

where $k = t_1 \cdot 1 + \cdots + t_n \cdot n$ and $\ell = s_1 \cdot 1 + \cdots + s_n \cdot n$ are the sums of the respective parts.

Proof. The only factor that needs explanation is the power of two. A cycle of length m can be given signs in 2^m ways, 2^{m-1} of which resulting in an even number of signs and 2^{m-1} of which in an odd number of signs.□

2.4 An algorithm for the cycle index of the hyperoctahedral group

We are now able to answer the question how many permutations in S_{2^n} of which cycle type are induced by the $2^n n!$ elements of $\mathcal{B}_n$ by implementing the following algorithm.

Algorithm 1: Counting and tabulating the induced permutations of $\mathcal{B}_n$.

Let $n \in \mathbb{N}$ be given.

Step 1. Generate the $\Delta(n)$ double partitions $(\tau_+, \tau_-) \vdash (k, \ell)$ of n.

Step 2. For each such double partition, construct a single $h \in \mathcal{B}_n$ with signed cycle type

$$t_{\pm}(h) = \left\{ \begin{array}{l} t_+(h) \\ t_-(h) \end{array} \right. = \left\{ \begin{array}{l} \tau_+ \\ \tau_- \end{array} \right.$$

and evaluate the expression in (18) to count how many of them there are.

Step 3. Compute the type $t(\pi_h)$ of the permutation $\pi_h \in S_{2^n}$ induced by h.

Step 4. Accumulate the result of Steps 2 and 3 over all double partitions in a table.

Example. The conjugacy classes of $\mathcal{B}_3$ are indexed by the ten double partitions of 3. Below we list these ten, and at their left we show how many elements of that type there are in $\mathcal{B}_3$.

$$1: \left\{ \begin{array}{c} (3,0,0) \\ (0,0,0) \end{array} \right. \quad 6: \left\{ \begin{array}{c} (1,1,0) \\ (0,0,0) \end{array} \right. \quad 8: \left\{ \begin{array}{c} (0,0,1) \\ (0,0,0) \end{array} \right. \quad 3: \left\{ \begin{array}{c} (2,0,0) \\ (1,0,0) \end{array} \right. \quad 6: \left\{ \begin{array}{c} (0,1,0) \\ (1,0,0) \end{array} \right.$$

$$1: \left\{ \begin{array}{c} (0,0,0) \\ (3,0,0) \end{array} \right. \quad 6: \left\{ \begin{array}{c} (0,0,0) \\ (1,1,0) \end{array} \right. \quad 8: \left\{ \begin{array}{c} (0,0,0) \\ (0,0,1) \end{array} \right. \quad 3: \left\{ \begin{array}{c} (1,0,0) \\ (2,0,0) \end{array} \right. \quad 6: \left\{ \begin{array}{c} (1,0,0) \\ (0,1,0) \end{array} \right.$$

Table 3 lists for each conjugacy class its cardinality, together with one element $h \in \mathcal{B}_3$ from that class, and the cycle type of its induced permutation π_h in S_8. It also illustrates Remark 2.4: elements from distinct conjugacy classes of $\mathcal{B}_3$ may induce permutations in S_8 the same cycle type. Table 4 groups them together. Note that instead of computing the cycle types of the induced permutations of all $2^n n!$ elements of $\mathcal{B}_n$, we need to compute only $\Delta(n)$ of them. ◊

The usual way in which the table in (4) is expressed, is as a *cycle index* polynomial [8, 27].

Table 3: Cycle types of induced permutations and their cardinality.

#	h	π_h	π_h	h	#
1	(1)(2)(3)	(8, 0, 0, 0, 0, 0, 0, 0)	(0, 4, 0, 0, 0, 0, 0, 0)	$(\overline{1})(\overline{2})(\overline{3})$	1
6	(1)(2 3)	(4, 2, 0, 0, 0, 0, 0, 0)	(0, 0, 0, 2, 0, 0, 0, 0)	$(\overline{1})(\overline{2}\ 3)$	6
8	(1 2 3)	(2, 0, 2, 0, 0, 0, 0, 0)	(0, 1, 0, 0, 0, 1, 0, 0)	$(\overline{1}\ 2\ 3)$	8
3	(1)(2)$(\overline{3})$	(0, 4, 0, 0, 0, 0, 0, 0)	(0, 4, 0, 0, 0, 0, 0, 0)	(1)$(\overline{2})(\overline{3})$	3
6	(1 2)$(\overline{3})$	(0, 4, 0, 0, 0, 0, 0, 0)	(0, 0, 0, 2, 0, 0, 0, 0)	(1)$(\overline{2}\ 3)$	6

Table 4: Cycle index of $\mathcal{B}_3$ in tabulated form.

#	π_h
1	(8, 0, 0, 0, 0, 0, 0, 0)
6	(4, 2, 0, 0, 0, 0, 0, 0)
13	(0, 4, 0, 0, 0, 0, 0, 0)
8	(2, 0, 2, 0, 0, 0, 0, 0)
12	(0, 0, 0, 2, 0, 0, 0, 0)
8	(0, 1, 0, 0, 0, 1, 0, 0)

Definition 2.12. The *cycle index* of the induced permutations on $\mathcal{B}_n$ of the hyperoctahedral group is the polynomial

$$Z_n(x_1, \ldots, x_\ell) = \frac{1}{|\mathcal{B}_n|} \sum_{h \in \mathcal{B}_n} \prod_{i=1}^{2\ell(n)} x_i^{t_i}. \tag{19}$$

Here, t_i is the i-th entry of $t(\pi_h)$ and ℓ is the *Landau function*, which assigns to n the largest order of an element from the symmetric group S_n. Its values

$$1, 1, 2, 3, 4, 6, 6, 12, 15, 20, 30, 30, 60, 60, 84, \ldots \tag{20}$$

can be found as sequence A000793 of the *Online Encyclopedia of Integer Sequences*.

Combining (4) and (19), the cycle index polynomial Z_3 of $\mathcal{B}_3$ can be found as

$$Z_3(x_1, x_2, x_3, x_4, x_5, x_6) = \frac{1}{48}\left(x_1^8 + 6x_1^4x_2^2 + 13x_2^4 + 8x_1^2x_3^2 + 12x_4^2 + 8x_2x_6\right). \tag{21}$$

Further explicit expressions for the cycle index polynomials Z_n of $\mathcal{B}_n$ can be found in the literature [11] only for $n \leq 6$. The above rather simple algorithm implemented on a personal computer can produce the table corresponding to Z_n of the form (36) for each $n \leq 10$ within a second. In the papers [10, 20], the cycle type $t(\pi_h)$ of the permutation $\pi_h \in S_{2^n}$ induced by h is expressed in terms of the signed cycle type of the signed permutation corresponding to $h \in \mathcal{B}_n$. Although algebraically of interest, their expressions are unfortunately too abstract to generate explicit numbers in a straightforward way. The above algorithm solves that problem.

3 The 0/1-polytopes in the unit n-cube

A 0/1-*polytope* [23] is the convex hull of a (possibly empty) subset $V \subset \mathbb{B}^n$. Since distinct subsets of $\mathbb{B}^n$ give rise to distinct 0/1-polytopes, we can and prefer to define a 0/1-polytope alternatively but equivalently as a map $c : \mathbb{B}^n \to \{0, 1\}$, using the obvious correspondence

$$c : \mathbb{B}^n \to \{0, 1\} : \quad v \mapsto 1 \Leftrightarrow v \in V. \tag{22}$$

Table 5: Doubly exponential growth of the number $|\mathcal{P}_n|$ of 0/1-polytopes in I^n.

n	0	1	2	3	4	5	6
$\lvert\mathcal{P}_n\rvert$	2	4	16	256	65536	4294967296	18446744073709551616

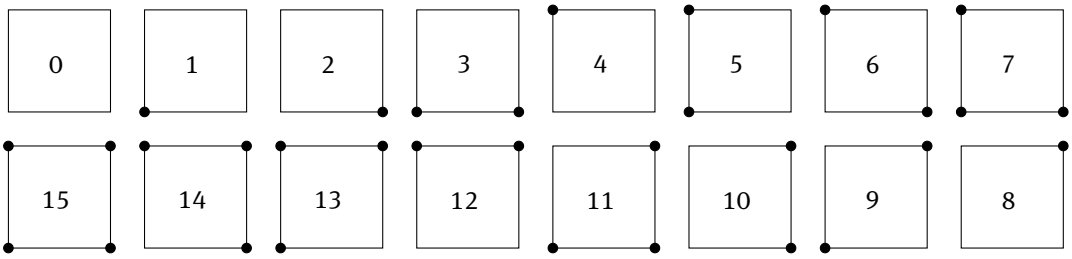

Figure 8: The sixteen 0/1-polytopes in I^2 and their numbering given in (24).

Such a map can be seen as a *two-coloring* of the vertices of I^n with "colors" 0 and 1. We denote the set of all maps $\mathbb{B}^n \to \{0,1\}$ by $\mathcal{P}_n$, and write $\mathcal{P}_n^k \subset \mathcal{P}_n$ for all $c \in \mathcal{P}_n$ with the property that precisely k elements of $\mathbb{B}^n$ are mapped to 1: these correspond to the 0/1-polytopes with exactly k vertices. Observe that

$$\mathcal{P}_n = \bigcup_{k=0}^{2^n} \mathcal{P}_n^k \quad \text{and} \quad |\mathcal{P}_n| = \sum_{k=0}^{2^n} \left|\mathcal{P}_n^k\right| = \sum_{k=0}^{2^n} \binom{2^n}{k} = 2^{2^n}. \tag{23}$$

The *double-exponential* growth of $|\mathcal{P}_n|$ in n is illustrated in the below table. Already for $n = 6$ it exceeds (by one) the number of grains of rice that the poor merchant claimed from the king in the legend of the chess board, as displayed in Table 5. We assign to each 0/1-polytope c the unique integer $\mathcal{N}(c)$ between 0 and $2^{2^n}-1$ given by

$$\mathcal{N}(c) = \sum_{v \in \mathbb{B}^n} c(v) 2^{\beta(v)}, \tag{24}$$

where β is the binary-to-decimal numbering of the vertices of $\mathbb{B}^n$ introduced in Section 2.

Example. Depicted below are the 0/1-polytopes c in the unit square. A circle is drawn around $v \in \mathbb{B}^2$ if and only if $c(v) = 1$. The number in the center of each square is $\mathcal{N}(c)$. Obviously, $\mathcal{N}(c) + \mathcal{N}(\tilde{c}) = 2^{2^n} - 1$ for *complementary* 0/1-polytopes, by which we mean polytopes c and $\tilde{c}$ such that $(c + \tilde{c})(v) = 1$ for all $v \in \mathbb{B}^n$.

3.1 Cube symmetries acting on 0/1-polytopes: 0/1-equivalence

Each element h of the hyperoctahedral group $\mathcal{B}_n$ induces a permutation H_h of $\mathcal{P}_n$ by $H_h : \mathcal{P}_n \to \mathcal{P}_n : c \mapsto c \circ h$. For each fixed k it restricts to a permutation of $\mathcal{P}_n^k \subset \mathcal{P}_n$. Via the numbering $\mathcal{N}$ defined in (24) it moreover induces a permutation

$$\Pi_h : \{0, \ldots, 2^{2^n} - 1\} \to \{0, \ldots, 2^{2^n} - 1\} : \quad k \mapsto \left(\mathcal{N} \circ H_h \circ \mathcal{N}^{-1}\right)(k). \tag{25}$$

It turns out to be of interest to know the cardinalities $|\mathcal{S}|$ and $|\mathcal{S}^k|$ of the sets

$$\mathcal{S} = \{(h, c) \in \mathcal{B}_n \times \mathcal{P}_n \quad | \quad c = c \circ h\} \quad \text{and} \quad \mathcal{S}^k = \{(h, c) \in \mathcal{B}_n \times \mathcal{P}_n^k \quad | \quad c = c \circ h\}. \tag{26}$$

Before explaining why, we present an example.

Example. For each of the eight $h \in \mathcal{B}_2$, the permutations Π_h of $\{0, \ldots, 15\}$ are given in Table 6. The (bold) fixed points correspond to $\mathcal{S}$, and are added up per row and per column. We see directly that $|\mathcal{S}| = 48$. After identifying the 0/1-polytopes with k vertices for given $k \in \{0, \ldots, 4\}$, we moreover find that $|\mathcal{S}^0| = 8$, $|\mathcal{S}^1| = 8$,

Table 6: The action of $\mathcal{B}_3$ on the sixteen 0/1-polytopes in I^2.

$\mathcal{B}_2 \times \mathcal{P}_2$	0	1	2	3	4	5	6	7	8	9	10	11	12	13	14	15	
id	**0**	**1**	**2**	**3**	**4**	**5**	**6**	**7**	**8**	**9**	**10**	**11**	**12**	**13**	**14**	**15**	16
c_1	**0**	2	1	**3**	8	10	9	11	4	6	5	7	**12**	14	13	**15**	4
c_2	**0**	4	8	12	1	**5**	9	13	2	6	**10**	14	3	7	11	**15**	4
$c_1 \circ c_2$	**0**	8	4	12	2	10	**6**	14	1	**9**	5	13	3	11	7	**15**	4
s_1	**0**	**1**	4	5	2	3	**6**	**7**	**8**	**9**	12	13	10	11	**14**	**15**	8
$s_1 \circ c_1$	**0**	4	1	5	8	12	9	13	2	6	3	7	10	14	11	**15**	2
$s_1 \circ c_2$	**0**	2	8	10	1	3	9	11	4	6	12	14	5	7	13	**15**	2
$s_1 \circ c_1 \circ c_2$	**0**	8	**2**	10	**4**	12	**6**	14	1	**9**	3	**11**	5	**13**	7	**15**	8
	8	2	2	2	2	2	4	2	2	4	2	2	2	2	2	8	48

(27)

$|\mathcal{S}^2| = 16$, $|\mathcal{S}^3| = 8$, and $|\mathcal{S}^4| = 8$.

It may decrease complexity and uncover structure when we consider all elements in the orbit $\mathcal{E}_n(c)$ of a 0/1-polytope c (elements in the same column of the above table) as equivalent.

Definition 3.1 (0/1-equivalence)**.** *Two* 0/1*-polytopes* $c, \tilde{c} \in \mathcal{P}_n$ *for which there exists an* $h \in \mathcal{B}_n$ *such that* $\tilde{c} = c \circ h$ *are called* 0/1-equivalent.

It is clear that 0/1-equivalence of 0/1-polytopes implies their congruence; however, the converse does not hold [23]. Thus, 0/1-equivalence is a finer type of equivalence than congruence.

We will now count the number ε_n of 0/1-equivalence classes of 0/1-polytopes. Since 0/1-equivalent 0/1-polytopes have the same number of vertices, we will count the number ε_n^k of 0/1-equivalence classes of 0/1-polytopes with k vertices, after which $\varepsilon_n = \sum_k \varepsilon_n^k$.

Lemma 3.2. *The number* ε_n^k *of* 0/1*-equivalence classes of* 0/1*-polytopes with* k *vertices equals*

$$\varepsilon_n^k = \sum_{c \in \mathcal{P}_n^k} \frac{1}{|\mathcal{E}_n(c)|} = \sum_{c \in \mathcal{P}_n^k} \frac{|\mathcal{S}_c|}{|\mathcal{B}_n|}, \quad \text{where} \quad \mathcal{S}_c = \{h \in \mathcal{B}_n \quad | \quad c = c \circ h\}. \tag{28}$$

Proof. Trivially, given $c \in \mathcal{P}_n^k$, all $\tilde{c} \in \mathcal{P}_n^k$ that belong to $\mathcal{E}_n(c)$ contribute one to the sum. This proves the first equality in (28). Next, if $h \in \mathcal{B}_n$ is such that $c \circ h = \tilde{c} = c$, then also $c \circ h_s \circ h = \tilde{c}$ if and only if $h_s \in \mathcal{S}_c$. Thus, for each $\tilde{c} \in \mathcal{E}_n(c)$ there are exactly $|\mathcal{S}_c|$ elements of $\mathcal{B}_n$ that map c onto $\tilde{c}$, proving the second equality. □

Corollary 3.3. *We have that*

$$\varepsilon_n^k = \frac{|\mathcal{S}^k|}{|\mathcal{B}_n|} \quad \text{and} \quad \varepsilon_n = \frac{|\mathcal{S}|}{|\mathcal{B}_n|} \quad \text{due to} \quad \sum_{c \in \mathcal{P}_n^k} |\mathcal{S}_c| = |\mathcal{S}^k| \quad \text{and} \quad \sum_{k=0}^{2^n} |\mathcal{S}^k| = |\mathcal{S}|. \tag{29}$$

Using this corollary we can continue to look at the example for $n = 2$.

Example (continued) Since for $n = 2$ there are 48 elements in $\mathcal{S}$, by Corollary 3.3 we find $48/8 = 6$ distinct 0/1-equivalence classes of 0/1-polytopes, being

$$\{0\}, \quad \{1, 2, 4, 8\}, \quad \{3, 5, 10, 12\}, \quad \{6, 9\}, \quad \{7, 11, 13, 14\} \quad \text{and} \quad \{15\}, \tag{30}$$

consisting of 0/1-polytopes with zero, one, two, two, three, and four vertices, respectively. For all the 0/1-polytopes with, for instance, two vertices, the fixed points add up to 16, confirming the existence of two distinct 0/1-equivalence classes in $\mathcal{P}_2^2$. ◊

3.2 Counting 0/1-polytopes invariant under a given cube symmetry

Counting the elements of $\mathcal{S}$ can be done by counting for each $c \in \mathcal{P}_n$ the number of elements of the set $\mathcal{S}_c$ from (28). Alternatively, one can also count for each $h \in \mathcal{B}_n$ the number of elements of the set

$$\mathcal{S}_h = \{c \in \mathcal{P}_n \quad | \quad c = c \circ h\}. \tag{31}$$

This is the Cauchy-Frobenius Lemma, also known as (not) Burnside's Lemma [8]. Note that counting $\mathcal{S}_c$ corresponds to counting the fixed points *per column* of the table in (27).

Proposition 3.4. *For given $h \in \mathcal{B}_n$, $c = c \circ h$ if and only if for each cycle of π_h, c is constant on the pre-image under β of all numbers in that cycle.*

As a consequence, the number of 0/1-polytopes that are invariant under a given $h \in \mathcal{B}_n$ with $t(\pi_h) = (t_1, \ldots, t_{2^n})$ equals the number of subsets of the set of the $t_1 + \cdots + t_{2^n}$ cycles of π_h.

Corollary 3.5. *Let $h \in \mathcal{B}_n$ be given with $t(\pi_h) = (t_1, \ldots, t_{2^n})$. Then the cardinality $|\mathcal{S}_h|$ of the set $\mathcal{S}_h$ equals $|\mathcal{S}_h| = 2^{t_1 + \cdots + t_{2^n}}$.*

Proof. According to Proposition 3.4, the numbers within the same cycle of π_h must either all be mapped to 0 or all be mapped to 1 by $c \circ \beta^{-1}$. □

The number of 0/1-polytopes *with k vertices* that are invariant under a given cube symmetry h equals the number of subsets of the set of $t_1 + \cdots + t_{2^n}$ cycles of π_h *whose lengths sum to k*.

Theorem 3.6. *Let $h \in \mathcal{B}_n$ be given with $\tau = t(\pi_h) = (t_1, \ldots, t_{2^n})$, and let $k \leq 2^n$. The cardinality $|\mathcal{S}_h^k|$ of the set $\mathcal{S}_h^k = \{c \in \mathcal{P}_n^k \quad | \quad c = c \circ h\}$ equals*

$$|\mathcal{S}_h^k| = \sum_{\kappa \vdash k} a(\tau, \kappa), \quad \text{where} \quad a(\tau, \kappa) = \prod_{j=1}^{k} \binom{t_j}{\kappa_j}, \tag{32}$$

and where the sum ranges over all integer partitions κ of k.

Proof. Let $(\kappa_1, \ldots, \kappa_k)$ be a partition of k. The number of ways that this partition can be selected from the partition $(t_1, \ldots, t_n)$ of n equals the product over all $j \in \{1, \ldots, k\}$ of the number of ways that κ_j cycles of length j can be selected from the t_j cycles of length j. □

Corollary 3.7. *The number of 0/1-equivalence classes of $\mathcal{P}_n^k$ equals*

$$\varepsilon_n^k = \frac{1}{|\mathcal{B}_n|} \sum_{h \in \mathcal{B}_n} \sum_{\kappa \vdash k} a(t(\pi_h), \kappa). \tag{33}$$

Example. Consider the induced permutation π_h of the vertices of I^3 with cycle type

$$t(\pi_h) = (4, 2, 0, 0, 0, 0, 0, 0), \tag{34}$$

which consists of $4 + 2 = 6$ cycles. Hence, the number of 0/1-polytopes that are mapped upon themselves by h equals $2^6 = 64$, which illustrates Corollary 3.5. To illustrate Theorem 3.6, consider the five partitions of $k = 4$, being $1 + 1 + 1 + 1 = 1 + 1 + 2 = 1 + 3 = 2 + 2 = 4$ and their corresponding cycle types,

$$(4, 0, 0, 0), \quad (2, 1, 0, 0), \quad (1, 0, 1, 0), \quad (0, 2, 0, 0), \quad (0, 0, 0, 1). \tag{35}$$

Only the first, second, and fourth partition contribute to the sum in (32), which evaluates to

$$\binom{4}{4}\binom{2}{0}\binom{0}{0}\binom{0}{0} + \binom{4}{2}\binom{2}{1}\binom{0}{0}\binom{0}{0} + \binom{4}{0}\binom{2}{2}\binom{0}{0}\binom{0}{0} = 14. \tag{36}$$

Thus, each $h \in \mathcal{B}_n$ with induced cycle type $t(\pi_h)$ as in (34), leaves invariant fourteen 0/1-polytopes in I^3 with four vertices. See also Table 5 in the next example.

Table 7: Computation of the numbers $a(\tau, \kappa)$.

					0	1	0	2	4	κ_1
					0	0	2	1	0	κ_2
					0	1	0	0	0	κ_3
					1	0	0	0	0	κ_4
12	0	0	0	2	**2**	**0**	**0**	**0**	**0**	24
8	0	1	0	0	**0**	**0**	**0**	**0**	**0**	0
13	0	4	0	0	**0**	**0**	**6**	**0**	**0**	78
8	2	0	2	0	**0**	**4**	**0**	**0**	**0**	32
6	4	2	0	0	**0**	**0**	**1**	**12**	**1**	84
1	8	0	0	0	**0**	**0**	**0**	**0**	**70**	70
48	t_1	t_2	t_3	t_4	24	32	84	72	76	288

(37)

3.3 An algorithm for counting the 0/1-equivalence classes of $\mathcal{P}_n^k$

Corollary 3.7 in combination with the considerations in Section 2 give a way to compute the number $|\mathcal{P}_n^k|$ of 0/1-equivalence classes of 0/1-polytopes with k vertices as follows.

Algorithm 2. Let integers n, k with $0 \le k \le 2^n$ be given.

(1) Use Algorithm 1 from Section 2.4 to generate the cycle index Z_n of $\mathcal{B}_n$ in tabulated form.

(2) Generate a second table with the $p(k)$ partitions of k, see for instance [25].

(3) For each cycle type $\tau = (t_1, \ldots, t_{2^n}) \vdash 2^n$ from the first table:

(a) sum the numbers $a(\tau, \kappa)$ from (32) over all $\kappa \vdash k$;

(b) multiply the result by the number of $h \in \mathcal{B}_n$ for which $t(\pi_h) = t$.

(4) Sum over all $\tau = (t_1, \ldots, t_{2^n}) \vdash 2^n$ from the first table.

To illustrate this algorithm, we perform it in detail in the example below.

Example. We consider the case $n = 3$ and $k = 4$. The part of Table 7 to the left of the 6×5 block in boldface is the table representing Z_3 from (4). The part of Table 7 above the boldface part contains the five partitions of 4. Note that only the values of $t_1, \ldots, t_4$ are needed to be able to compute each of the numbers $a(\tau, \kappa)$. The numbers 1, 12, 1 in the fifth row in boldface are the ones computed in (36) of the previous example. The sum 288 of the numbers in the 6×5 block divided by the order 48 of $\mathcal{B}_3$ equals 6, indeed the number of nonequivalent 0/1-tetrahedra in the cube, including two degenerate ones, as depicted in Figure 9.

Remark 3.8. The combinatorial road [8, 27] to arrive at the same result is to substitute in the cycle index polynomial Z_n of $\mathcal{B}_n$ in (19) the expressions $x_i = b^i + w^i$. Then the coefficient of the monomial $w^k b^{2^n-k}$ in the expansion equals $|\mathcal{P}_n^k|$. Although theoretically elegant and valuable, and widely applicable, it is not very suited for computing concrete numerical values.

The methodology described in Sections 2 and 3 leads to a way to compute the *number* of 0/1-polytopes in I^n modulo the symmetries of I^n. See also Section 6 for some explicitly computed values. It does not yield a *specific element* from each 0/1-equivalence class. In the next section we will investigate this *enumeration problem*.

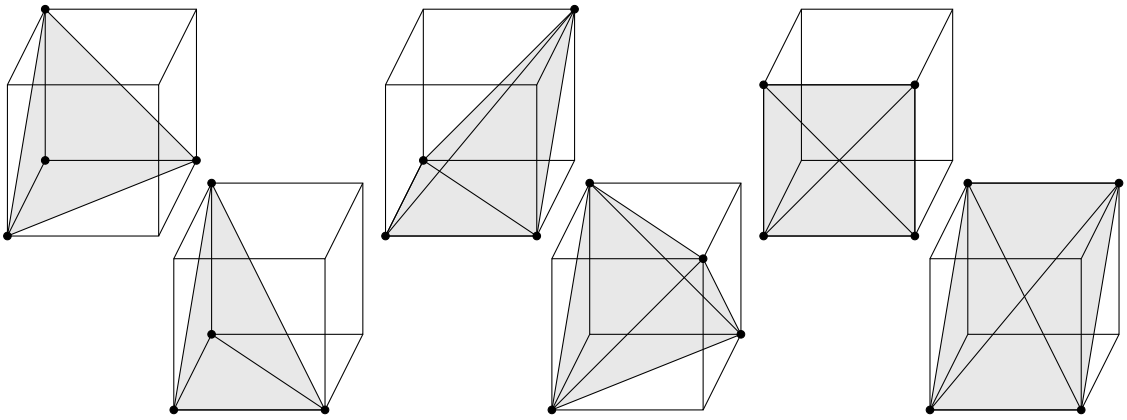

Figure 9: Representatives of each of the six 0/1-equivalence classes of all 0/1-tetrahedra.

4 Minimal matrix representations of 0/1-polytopes

We will now designate in each 0/1-equivalence class $\mathcal{E}_n(c)$ of a 0/1-polytope c some special *representatives*. One of them we denote as the *minimal representative* from that equivalence class. Obvious candidates for such minimal representatives are the 0/1-polytopes c for which

$$\mathcal{N}(c) \leq \mathcal{N}(c \circ h) \quad \text{for all } h \in \mathcal{B}_n, \tag{38}$$

where $\mathcal{N}$ is the numbering defined in (24). However, with this definition it may happen that $c \in \mathcal{P}_n^k$ is a minimal representative, whereas none of its facets in $\mathcal{P}_n^{k-1}$ is minimal. For computational purposes, we prefer a minimal representative to have that property.

4.1 Matrix representations of 0/1-polytopes

A natural way to represent a 0/1-polytope c, alternative to a mapping $c : \mathbb{B}^n \to \{0, 1\}$, is by means of 0/1-matrices whose colums are the vertices of c.

Definition 4.1 (Matrix representation)**.** If the columns of a matrix P of size $n \times k$ are precisely the k distinct vertices of a 0/1-polytope $c \subset \mathcal{P}_n^k$, we will call P a *matrix representation* of c. With each matrix representation P we associate the integer vectors

$$v(P) = v_n^\top P \Pi_1 \quad \text{and} \quad \mu(P) = \Pi_2 P w_k \tag{39}$$

where

$$v_n^\top = \left(2^0, 2^1, \ldots, 2^{n-1}\right) \quad \text{and} \quad w_k^\top = \left(2^{k-1}, \ldots, 2^1, 2^0\right) \tag{40}$$

and where Π_1 is the *unique* $k \times k$ column permutation matrix sorting the k entries of $v_n^\top P \Pi_1$ from left to right in *increasing order*, and Π_2 *any* $n \times n$ row permutation matrix sorting the n possibly non-distinct entries of $\Pi_2 P w_k$ from top to bottom in *non-increasing* order.

The permutations Π_1, Π_2 depend on P, but this dependence is suppressed from the notation. As P has distinct columns, each $c \in \mathcal{P}_n^k$ has exactly $k!$ distinct matrix representations.

Proposition 4.2. *The following statements are equivalent:*

(1) *P_1 and P_2 are matrix representations of the same 0/1-polytope $c \in \mathcal{P}_n^k$;*

(2) *there exists a $k \times k$ permutation matrix Π such that $P_1 = P_2 \Pi$;*

(3) $v(P_1) = v(P_2)$.

Proof. This follows from the fact that no vertex of I^n is a convex combination of other vertices of I^n, hence 0/1-polytopes are uniquely determined by their vertex set. □

Due to the equivalence (1) ⇔ (3) in Proposition 4.2, and with a slight abuse of notation, we will use $v(c)$ also for a 0/1-polytope $c \in \mathcal{P}_n$, and assign to it the vector $v(c)$ taken by any matrix representation P of c. Note that $v : \mathcal{P}_n \to \{0, \dots, 2^n\}^k$ is injective.

For given $c \in \mathcal{P}_n^k$, we will write $\mathcal{M}(c)$ for the set of all matrix representations of all $\tilde{c} \in \mathcal{E}_n(c)$. This induces an equivalence relation on the set $\mathcal{Z}$ of all matrix representations of 0/1-polytopes, that we will denote by $P_1 \sim P_2$. Before studying this equivalence on $\mathcal{Z}$, we introduce two simpler relations.

Definition 4.3 (Row complementation/permutation)**.** A 0/1-matrix P_2 is a *row complementation* of P_1, denoted by $P_2 \overset{c}{\sim} P_1$, if it results from P_1 after exchanging the zeros and ones in a subset of its rows; it is a *row permutation* of P_1, denoted by $P_2 \overset{p}{\sim} P_1$ if there exists a permutation matrix Π such that $P_2 = \Pi P_1$. □

Both $\overset{c}{\sim}$ and $\overset{p}{\sim}$ are equivalence relations on $\mathcal{Z}$. The 2^n row complementations applied to a given $P \in \mathcal{Z}$ result in matrix representations of each of the 0/1-polytopes in an orbit under the action of the subgroup $\mathcal{B}_n^c \subset \mathcal{B}_n$, whereas the $n!$ row permutations of P are matrix representations of those in an orbit under the action of the subgroup $\mathcal{B}_n^p \subset \mathcal{B}_n$. Thus, following Section 2, a matrix representation of each 0/1-polytope that is in the same 0/1-equivalence class of a given $c \in \mathcal{P}_n^k$ can be obtained by performing each of the $2^n n!$ combined row complementations and permutations to a given matrix representation P of c.

4.2 Verification of 0/1-equivalence $P_1 \sim P_2$ of matrix representations

For given $P_1, P_2 \in \mathbb{B}^{n\times k}$ let $r_1 = P_1 w_k$ and $r_2 = P_2 w_k$, where w_k is the vector from (40). If $P_1 \overset{c}{\sim} P_2$, then the j-th entries of r_1 and r_2 are equal in case the j-th rows of P_1 and P_2 are equal, and add up to $2^k - 1$ in case these rows are complementary. Hence, verification whether $P_1 \overset{c}{\sim} P_2$ can be done in at most $\mathcal{O}(nk)$ operations, which is dominated by the costs of computing r_1 and r_2. Verifying whether $P_1 \overset{p}{\sim} P_2$ asks to inspect if the n-vector r_1 is a permutation of r_2, requiring $\mathcal{O}(nk + n \log n)$ operations.

The combination of these two observations yields the following, which can be seen as a variant of stating that r_1 is a signed permutation of r_2, see Section 2.2.

Proposition 4.4. *Let $P_1, P_2 \in \mathcal{Z}$. There exists an $R \in \mathbb{B}^{n\times k}$ such that*

$$P_1 \overset{p}{\sim} R \overset{c}{\sim} P_2 \tag{41}$$

if and only if the $2n$ entries of the two n-vectors r_1 and $(2^k - 1)e - r_1$ are a permutation of the $2n$ entries of the two n-vectors r_2 and $(2^k - 1)e - r_2$.

The verification if $P_1 \overset{p}{\sim} R \overset{c}{\sim} P_2$ requires $\mathcal{O}(nk + 2n \log(2n)) = \mathcal{O}(nk + n \log n)$ operations.

Example. Consider matrices P_1 and P_2, with $r_1 = P_1 w_4$ and $r_2 = P_2 w_4$ computed as

$$P_1 w_4 = \begin{bmatrix} 0 & 1 & 1 & 0 \\ 0 & 0 & 1 & 0 \\ 0 & 0 & 0 & 1 \end{bmatrix} \begin{bmatrix} 8 \\ 4 \\ 2 \\ 1 \end{bmatrix} = \begin{bmatrix} 6 \\ 2 \\ 1 \end{bmatrix} \quad \text{and} \quad P_2 w_4 = \begin{bmatrix} 0 & 1 & 1 & 0 \\ 1 & 1 & 1 & 0 \\ 1 & 1 & 0 & 1 \end{bmatrix} \begin{bmatrix} 8 \\ 4 \\ 2 \\ 1 \end{bmatrix} = \begin{bmatrix} 6 \\ 14 \\ 13 \end{bmatrix}.$$

Then $P_1 \overset{c}{\sim} R \overset{p}{\sim} P_2$ for some $R \in \mathbb{B}^{3\times 4}$, because the entries $(6, 2, 1, 9, 13, 14)$ of the two 3-vectors r_1 and $15e - r_1$ can be permuted into the entries $(6, 14, 13, 9, 1, 2)$ of r_2 and $15e - r_2$. Indeed, P_2 is obtained by exchanging and complementing the second and third row of P_1.

Proposition 4.2 showed that if P_1 and P_2 are matrix representations of *the same* 0/1-polytope, then $P_1 = P_2\Pi$ for a permutation matrix Π that can be found by inspecting if $s_1 = v_n^\top P_1$ is a permutation of $s_2 = v_n^\top P_2$, with v_n from (40). To verify if $P_1 \sim P_2$, or in other words, if P_2 is a *column permutation* of a row complementation and row permutation of P_1, is computationally much more complex.

Proposition 4.5. *Let $P_1, P_2 \in \mathcal{Z}$. Then $P_1 \sim P_2$ if and only if there exists an $R \in \mathcal{Z}$ and a permutation matrix Π such that*

$$P_1 \overset{p}{\sim} R \overset{c}{\sim} P_2\Pi, \tag{42}$$

the verification of which can be done in $\mathcal{O}(k!(nk + n\log n))$ operations.

Proof. The verification can be done by looping over all $k!$ permutation matrices Π and performing the verification in Proposition 4.4 for each of them. □

Remark 4.6. Relation (42) holds if there exist permutation matrices Π_1 and Π_2 such that

$$\Pi_1 P_1 \overset{c}{\sim} P_2\Pi_2. \tag{43}$$

This more symmetric formulation suggests that in order to verify if $P_1 \sim P_2$, one can establish the existence of permutation matrices Π_1 and Π_2 such that $\Pi_1 P_1 \overset{c}{\sim} P_2\Pi_2$ in two ways:

- for each Π_2, verify if there exists Π_1 such that $\Pi_1 P_1 \overset{c}{\sim} P_2\Pi_2$;
- for each Π_1, verify if there exists Π_2 such that $\Pi_1 P_1 \overset{c}{\sim} P_2\Pi_2$.

The second strategy would require an efficient way to verify the existence of a *column* permutation of P_2 such that it equals a row complementation of the given matrix $\Pi_1 P_1$. This verification is far less trivial than the one in Proposition 4.4. Nevertheless, if $k > n + 1$, there are ways to repair this and make the second strategy more economic than the first. Because our main interest is 0/1-*simplices* for which $k \le n + 1$, we will not go into detail.

4.3 Minimal matrix representations and their properties

The lexicographical order $\prec$ on the integer vectors $v(P)$ associated with the matrix representations P of 0/1-polytopes $c \in \mathcal{P}_n$ induces a total order on $\mathcal{P}_n$ as well as on $\mathcal{Z}$.

Definition 4.7 (Minimal representative)**.** The *minimal representative* of a $c \in \mathcal{P}_n^k$ in $\mathcal{E}_n(c)$ is the unique 0/1-polytope $c^\star \in \mathcal{E}_n(c)$ for which $v(c^\star) \prec v(d)$ for all $d \in \mathcal{E}_n(c^\star)$, $d \neq c^\star$.

The minimal representative $c^\star$ of $c \in \mathcal{P}_n^k$ has $k!$ distinct matrix representations, of which we designate one as the minimal matrix representation.

Definition 4.8 (Minimal matrix representation)**.** The *minimal matrix representation* of $c \in \mathcal{P}_n$ in $\mathcal{M}(c)$ is the unique matrix representation $P^\star$ of $c^\star$ for which $v_n^\top P^\star = v(P^\star)$, in other words, whose column numbers $v_n^\top P^\star$ are strictly increasing.

We will now study further properties of minimal matrix representations of 0/1-equivalence classes of 0/1-polytopes. The following result proves a desirable property, mentioned already at the beginning of this section.

Lemma 4.9. *Let $P^\star$ be a minimal matrix representation of a 0/1-polytope $c \in \mathcal{P}_n^k$. Then for each $j \in \{1, \dots, k-1\}$, the submatrix $P_j^\star$ of $P^\star$ consisting of its j leftmost columns is a minimal matrix representation of a 0/1-polytope $c_j \in \mathcal{P}_n^j$.*

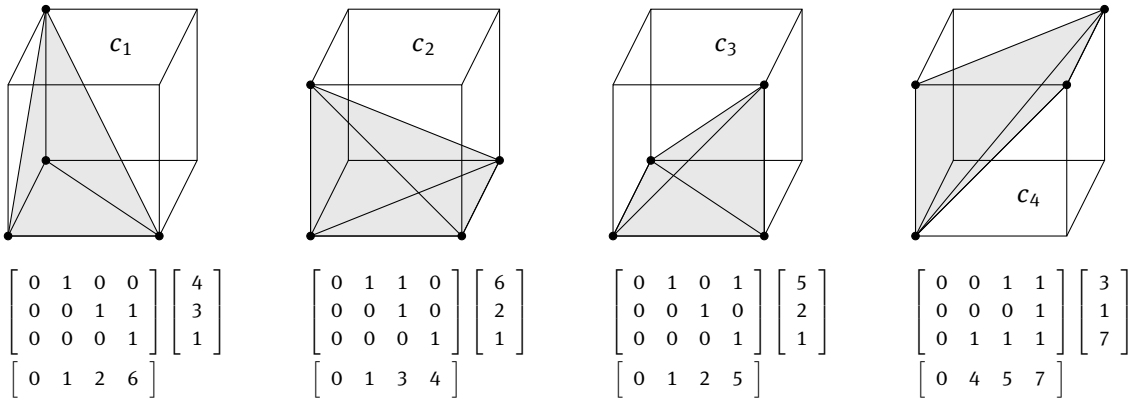

Figure 10: Four $0/1$-equivalent $0/1$-tetrahedra with corresponding matrix representations.

Proof. Let $P^\star \in \mathbb{B}^{n\times k}$ be a minimal matrix representation. Then by Definition 4.8, $v_n^\top P^\star$ is increasing, and hence, so is $v_n^\top P^\star_{k-1}$. To arrive at a contradiction, assume that $P^\star_{k-1}$ is not a minimal matrix representation. Then there exists a row permutation Π such that $\Pi P^\star_{k-1} \overset{c}{\sim} P_{k-1}$ and $v(P_{k-1}) \prec v(P^\star_{k-1})$. But this means that $\Pi P^\star \overset{c}{\sim} P$, where P is a matrix whose $k-1$ leftmost columns equal P_{k-1}. Irrespective of the rightmost column of P, this implies that $v(P) \prec v(P^\star)$, contradicting the minimality of $P^\star$. This proves that $P^\star_{k-1}$ is a minimal matrix representation, and hence inductively, the minimality of all $P^\star_j$. □

Corollary 4.10. *Any minimal representative of a* $0/1$*-polytope with* k *vertices contains a minimal representative of a* $0/1$*-polytope with* $k-1$ *vertices.*

Corollary 4.11. *The first column of a minimal matrix representation* $P^\star$ *of a* $0/1$*-polytope* $c \in \mathcal{P}_n^k$ *equals* $0 \in \mathbb{R}^n$.

Proof. According to Lemma 4.9, the first column of $P^\star$ is a minimal matrix representation of a $0/1$-polytope with one vertex. Obviously, this is the zero vector. □

By Definition 4.7, $v(P^\star) = v_n^\top P^\star$, which means that the integer vector $v_n^\top P^\star$ is increasing. The next lemma proves that additionally, $P^\star w_p$ is non-increasing from top to bottom.

Lemma 4.12. *Let* $P^\star$ *be a minimal matrix representation of a* $0/1$*-polytope* $c \in \mathcal{P}_n^k$. *Then*

$$P^\star w_k = \mu(P^\star) \tag{44}$$

or equivalently, $P^\star w_k$ *is non-increasing from top to bottom.*

Proof. Write $p_i^\star$ for row i of $P^\star$ and $p_j^\star$ for row j of $P^\star$. Assume that $1 \le i < j \le n$ and $p_i^\star w_k < p_j^\star w_k$, contradicting the statement to prove. Then

$$p = \min_{\ell\in\{1,\dots,k\}} \left\{ p_i^\star e_\ell \neq p_j^\star e_\ell \right\} \tag{45}$$

exists and equals the index of the leftmost column in which $p_i^\star$ and $p_j^\star$ differ. The assumption $p_i^\star w_k < p_j^\star w_k$ implies that $p_i^\star e_k = 0$ and $p_j^\star e_k = 1$. Write P for the matrix that results after the transposition of rows i and j of $P^\star$. Then the first $p-1$ columns of $P^\star$ and P coincide. However, in column p, the one in row j is exchanged with the zero in row i above it. As a result, $v_n^\top P \prec v_n^\top P^\star$, contradicting that $P^\star$ is a minimal matrix representation. □

In Figure 10 we display four elements $c_1, \dots, c_4$ from $\mathcal{E}_3(c_1)$ of the tetrahedron c_1 from Figure 5. The stabilizer $\mathcal{S}_{c_1}$ of c_1 in $\mathcal{B}_3$ contains two elements, hence $|\mathcal{E}_3(c_1)| = 24$. We also display matrix representations for $c_1, \dots, c_4$, all with increasing column numbers. Without proof, we mention the following facts for illustration.

• $\mathcal{N}(c_2) \le \mathcal{N}(c)$ for all $c \in \mathcal{E}_3(c_1)$, but none of its triangular facets is $\mathcal{N}$-minimal;

• c_3 is the unique minimal representative of $\mathcal{E}_3(c_1)$;

• $\mu(c_4)$ is not nonincreasing, hence c_4 is not the minimal representative of $\mathcal{E}_3(c_1)$;

• no 0/1-polytope formed by two or three vertices of c_4 is a minimal representative;

• c_1 has all properties proved above of the minimal representative, but is not it.

Now, let P be any matrix representation of a 0/1-simplex c with $k \le n+1$ vertices. For each $j \in \{1, \dots, k\}$, write P_j for the matrix obtained from P by first complementing those rows in P that have an entry 1 in column j, and then swapping columns 1 and j of the result. Each matrix P_j corresponds to c with one of its vertices placed at the origin. Hence, due to Corollary 4.11, there exists a $j \in \{1, \dots, k\}$ such that

$$P^\star = \Pi_1 P_j \Pi_2$$

for some permutation matrices Π_1 and Π_2, and where Π_2 leaves the first column of P_j invariant. Instead of applying all the $n!(k-1)!$ permutations and verifying which of them result in $P^\star$, we can use that by Lemma 4.12, the row numbers $P^\star w_k$ are non-increasing. Therefore, for each of the $(k-1)!$ choices for Π_2, it suffices to simply sort the rows of $P_j\Pi_2$. Then $P^\star$ must be among the resulting $k(k-1)! = k!$ matrices, $(k-1)!$ for each value of $j \in \{1, \dots, k\}$.

Summarized in algorithmic form, this reads as follows.

Algorithm 3: Computing the minimal matrix representation $P^\star$ of a 0/1-simplex c.

Let P be any matrix representation of c. Define $P_1, \dots, P_k$ as described above.

For $j = 1, \dots, k$;

(1) apply all $(k-1)!$ column permutations Π_2 to P_j that leave its first column invariant;

(2) for each of those, apply any row permutation Π_1 for which $\Pi_1 P_j \Pi_2 w_p$ is non-increasing;

(3) store the matrix $P_j^\star = \Pi_1 P_j \Pi_2$ for which $\Pi_1 P_j \Pi_2 w_p$ is lexicographically minimal.

Each $P_j^\star$ can be seen as a *local minimizer* over all matrices that can be obtained from P_j by permuting its rows and columns. The minimal among all k local minima is then $P^\star$.

Corollary 4.13. *A 0/1-polytope with k vertices has at most $k!$ distinct matrix representations P with $Pe_1 = 0$ and with Pw_k nonincreasing.*

We will now use Algorithm 3 to enumerate the minimal representatives and their minimal matrix representations of all 0/1-*triangles* in I^n, and in particular of the subset of all *acute* 0/1-triangles. These minimal matrix representations of 0/1-triangles will be extended by a computer code to minimal matrix representations of nonobtuse and acute 0/1-*simplices*.

4.4 The set of all minimal matrix representations of 0/1-triangles

Let $\mathcal{T} \in \mathcal{P}_n^3$ be a 0/1-triangle. We will characterize its minimal matrix representation $T^\star$. By Definition 4.8, we know that $v_n^\top T^\star$ is increasing; by Corollary 4.11, the first column of $T^\star$ equals zero; and by Lemma 4.12, $T^\star w_3$ is non-increasing. Therefore, we know that

$$T^\star = \left[\begin{array}{c|ccc} a & 0 & 1 & 1 \\ b & 0 & 1 & 0 \\ c & 0 & 0 & 1 \\ d & 0 & 0 & 0 \end{array}\right] \quad \text{for certain} \quad a+b+c+d = n, \tag{46}$$

and where the right-hand side stands for the $n \times 3$ matrix whose top a rows equal $[\,0\ 1\ 1\,]$, whose next b rows equal $[\,0\ 1\ 0\,]$ and so on. Of course, $T^\star$ is not minimal for *all* values of a, b, c, d. For instance, if $b > c$ it is

not. In that case, swapping the second and third column of $T^\star$ and sorting the rows, leads to a matrix with a smaller second column number: $2^{a+c} < 2^{a+b}$.

To further specify a, b, c, d, we compute the $k! = 6$ matrices that are generated by Algorithm 3, with start matrix $T_1^\star = T^\star$ for some choice of a, b, c, d. Each of those six matrices is of the same form as in (46), but with the numbers a, b, c, d of repeated rows permuted. Instead of writing down the matrices, we only present in Table 8 their corresponding permutations of a, b, c, d, in three sets of two, each pair belonging to one of the matrices $T_1^\star, T_2^\star, T_3^\star$, where $T_1^\star = T$,

Table 8: Induced (block-)permutations.

a	a	b	b	c	c
b	c	a	c	a	b
c	b	c	a	b	a
d	d	d	d	d	d

(47)

Observe that Table 8 basically consists, in fact, of all six permutations of a, b, c.

Theorem 4.14. *The matrix $T^\star$ is the minimal matrix representation of a 0/1-triangle $\mathcal{T}$ in I^n if and only if it is of the form (46) with*

$$1 \le a + b \quad \text{and} \quad a + b + c \le n \quad \text{and} \quad a \le b \le c. \tag{48}$$

Proof. Consider the column numbers of $T^\star$,

$$v_n^\top T_{11} = \left(0, \quad 2^{a+b} - 1, \quad 2^{a+b+c} - 2^{a+b} + 2^a - 1\right). \tag{49}$$

Necessary and sufficient conditions for this vector to be lexicographically minimal over all permutations of a, b, c are as follows. The second entry is minimal if and only if $a + b \le a + c$ and $a + b \le b + c$, hence if and only if $b \le c$ and $a \le c$. If this is the case, additionally the third entry is minimal if and only if $a \le b$. The fact that $a + b + c$ must be bounded above by n is trivial. The additional bound $1 \le a + b$ is a necessary and sufficient condition for the three vertices of $\mathcal{T}$ to be distinct. □

Corollary 4.15. *Let $T^\star$ be a minimal matrix representation of a 0/1-triangle $\mathcal{T}$ in I^n. Then:*

- *if $a = 0$ then $\mathcal{T}$ is a right triangle;*
- *if $a > 0$ then $\mathcal{T}$ has acute angles only.*

Proof. Suppose that $a = 0$. Then due to $1 \le a + b$ and $a \le b \le c$ in (48), we have that $1 \le b$ and $1 \le c$ and thus, $T^\star$ in (46) obviously represents a nondegenerate right triangle. If $0 < a$, then again due to (48), also $0 < b \le c$. This shows that the difference between the second and third column is not orthogonal to either one of them, and thus is $T^\star$ not right. Finally, since no triangle in I^n can have obtuse angles, also the second bullet is proved. □

Theorem 4.14 establishes a bijection between the minimal matrix representations of all 0/1-triangles in I^n and the set all points (except the origin due to $1 \le a + b$) with integer coordinates in the polyhedron K in the nonnegative octant of $\mathbb{R}^3$ defined by the inequalities

$$0 \le a, \quad 0 \le b, \quad 0 \le c \quad \text{and} \quad a + b + c \le n \quad \text{and} \quad a \le b \le c. \tag{50}$$

A closer inspection shows that K is a tetrahedron, the intersection of the so-called *path-tetrahedron* P defined by the inequalities $0 \le a \le b \le c \le n$, and the *cube-corner* C defined by $0 \le a$, $0 \le b$, $0 \le c$ and $a + b + c \le n$. This is depicted in Figure 11.

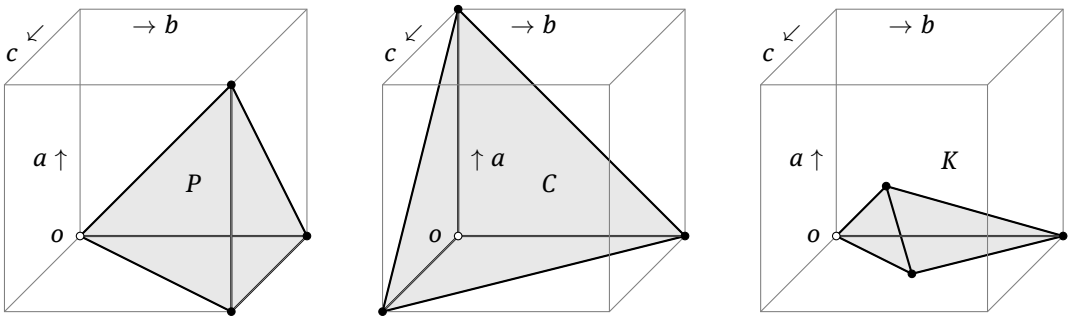

$P:\ 0 \le a \le b \le c \le n$ and $C:\ a+b+c \le n$ $K = P \cap C$

Figure 11: The tetrahedron K as intersection a path tetrahedron P and a cube corner C.

Table 9: Right, acute, and all 0/1-triangles in I^n modulo the action of $\mathcal{B}_n$.

n	2	3	4	5	6	7	8	9	10	11	12	13	14	15	16	17	18	19	20
r_n	1	2	4	6	9	12	16	20	25	30	36	42	49	56	64	72	81	90	100
a_n	0	1	2	4	7	11	16	23	31	41	53	67	83	102	123	147	174	204	237
d_n	1	3	6	10	16	23	32	43	56	71	89	109	132	158	187	219	255	294	337

Remark 4.16. The *right* triangles correspond to the integer points in the bottom facet of K.

Because the cube $[0, n]^3$ can be subdivided into six congruent path tetrahedra all sharing the same long diagonal, K is one of six congruent parts of the cube corner. In fact, each of those six parts corresponds to exactly one of the matrices in Table 6. Obviously, with the above characterizations, the enumeration of all minimal matrix representations of all 0/1-triangles, or of those of all acute 0/1-triangles is now a trivial matter.

In [2] we derived explicit formulas for all, all right, and all acute 0/1-triangles in an alternative way. We include the results here for completeness.

Proposition 4.17. *The number of* 0/1*-equivalence classes of right triangles in* I^n *equals*

$$\left\lfloor \frac{n}{2} \right\rfloor \left\lceil \frac{n}{2} \right\rceil . \tag{51}$$

The number of 0/1*-equivalence classes of acute triangles in* I^n *equals*

$$\left\lfloor \frac{2n^3 + 3n^2 - 6n + 9}{72} \right\rfloor . \tag{52}$$

In Table 9 are listed the numbers r_n and a_n of 0/1-equivalence classes of right and acute 0/1-triangles and their sum d_n for small values of n. In the OEIS, the sequence r_n has label A002620, sequence a_n has label A181120, and d_n has label A034198. Only the latter has as description "number of distinct triangles on vertices of n-dimensional cube", the other two are not associated with counting triangles in I^n.

5 Generating minimal representatives of acute 0/1-simplices

We will now describe how to generate by means of a computer program minimal matrix representations of each 0/1-equivalence class of so-called *acute* 0/1*-simplices*, which are 0/1-simplices having only acute di-

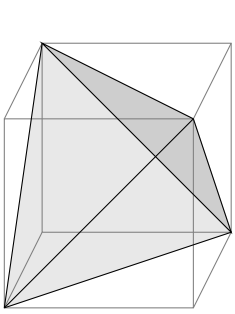

$$R_3^\star = [0 \mid P_3] = \left[\begin{array}{c|ccc} 0 & 1 & 1 & 0 \\ 0 & 1 & 0 & 1 \\ 0 & 0 & 1 & 1 \end{array}\right]$$

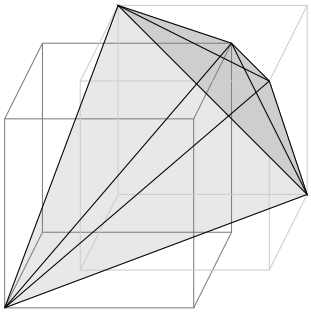

$$R_4^\star = [0 \mid P_4] = \left[\begin{array}{c|ccc} 0 & 1 & 1 & 1 \\ 0 & 1 & 0 & 0 \\ 0 & 0 & 1 & 0 \\ 0 & 0 & 0 & 1 \end{array}\right]$$

Figure 12: An acute antipodal n-simplex for $n = 3$ (left) and $n = 4$ (right) together with their minimal matrix representations $R_3^\star$ and $R_4^\star$ and their nonsingular parts P_3 and P_4 that satisfy the conditions in Definition 5.1.

hedral angles. They form the higher dimensional generalizations of the *acute* 0/1-*triangles* from the previous section.

Definition 5.1 (Acute k-simplex)**.** Let $c \in \mathcal{P}_n^k$ with $1 \le k \le n$ be a nondegenerate k-simplex in I^n. Let $R^\star \in \mathbb{B}^{n\times(k+1)}$ be the minimal matrix representation of c. Let P be the $n \times k$ matrix with the nonzero columns of $R^\star$. If the $k \times k$ Gramian $G = P^\top P$ satisfies:

(a) each off-diagonal entry of G^{-1} is negative (G^{-1} is *strictly Stieltjes*),

(b) each row sum of G^{-1} is positive (G^{-1} is *diagonally dominant*),

then c is called an *acute* 0/1-k-simplex.

The properties (a) and (b) are purely *geometric*, and concern the *dihedral angles* of the simplex, for which we refer to [6, 7] for details. These angles are invariant under the action of $\mathcal{B}_n$. This guarantees that the concept of acute 0/1-simplex is well-defined using only the minimal matrix representation. Note that G is invertible as c is assumed nondegenerate.

As examples of acute simplices, in Figure 12 we display on the left the *only* acute 0/1-*tetrahedron* in I^3, which is the regular one, and on the right the *only* acute 0/1-4-*simplex* in I^4, which is not regular. Both are members of the family of so-called *antipodal* simplices in I^n. An antipodal n-simplex in I^n is 0/1-equivalent with the simplex whose vertices are the origin and all $v \in \mathbb{B}^n$ with exactly one entry equal to zero. For this family, the matrices P and G from Definition 5.1 are, indexed by n,

$$P_n = \left[\begin{array}{c|c} e & 0 \\ \hline I_{n-1} & e \end{array}\right], \quad \text{and} \quad G_n = I_n + ee^\top + (n-3)e_n e_n^\top. \tag{53}$$

As before, e is the all-ones vector of appropriate length and I_ℓ is the $\ell \times \ell$ identity matrix. It is easy to verify that G^{-1} satisfies the criteria (a) and (b) in Definition 5.1 for the family of antipodal simplices to be acute.

Remark 5.2. The tetrahedral facet T of the antipodal 4-simplex represented by the first four columns K of the matrix $R_4^\star$ is *congruent* to the regular tetrahedron in the left picture. They are, however, not 0/1-*equivalent*. Indeed, T does not lie in a three-dimensional cubic facet of I^4, and this property is invariant under the action of $\mathcal{B}_4$. A congruence Q mapping one onto the other is, for instance,

$$QK = \frac{1}{2}\begin{bmatrix} 1 & 1 & 1 & -1 \\ 1 & 1 & -1 & 1 \\ 1 & -1 & 1 & 1 \\ -1 & 1 & 1 & 1 \end{bmatrix}\left[\begin{array}{c|ccc} 0 & 1 & 1 & 1 \\ \hline 0 & 1 & 0 & 0 \\ 0 & 0 & 1 & 0 \\ 0 & 0 & 0 & 1 \end{array}\right] = \left[\begin{array}{c|ccc} 0 & 1 & 1 & 0 \\ 0 & 1 & 0 & 1 \\ 0 & 0 & 1 & 1 \\ \hline 0 & 0 & 0 & 0 \end{array}\right] \tag{54}$$

but this congruence Q is not a member of $\mathcal{B}_4$.

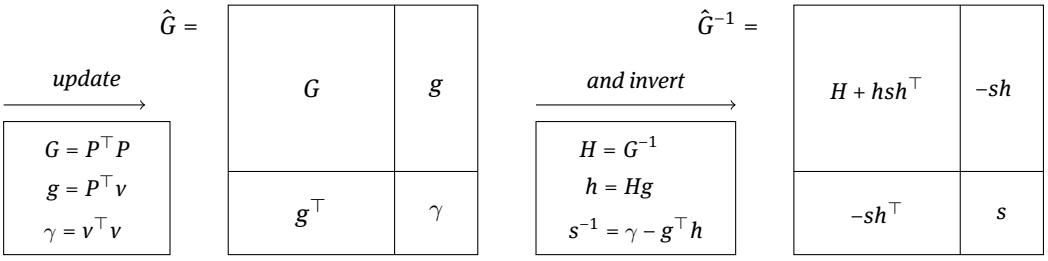

Figure 13: Updating the inverse of an updated Gramian.

5.1 Acute 0/1-simplices and their candidate acute extensions

Here we will list a number of properties of acute simplices that are relevant in the context of their computational enumeration. Some of them are new, others are simply valid for acute simplices in general [6, 7, 16].

Proposition 5.3 ([16])**.** *Each ℓ-facet of an acute 0/1-k-simplex is an acute 0/1-ℓ-simplex.*

This corresponds to the well-known linear algebraic statement that the inverse of each principal $k \times k$ submatrix of G is also a diagonally dominant strictly Stieltjes matrix. Together with Lemma 4.9, this proves the following.

Corollary 5.4. *Let $P^\star$ be the minimal matrix representation of an acute simplex $c \in \mathcal{P}_n^k$. Then for each $j \in \{1, \dots, k-1\}$, the submatrix $P_j^\star$ of $P^\star$ consisting of its j leftmost columns is a minimal matrix representation of an acute simplex $c_j \in \mathcal{P}_n^j$.*

Corollary 5.4 shows in particular that the first three columns of any minimal matrix representation of an acute 0/1-simplex form a minimal matrix representation of an acute 0/1-triangle.

Definition 5.5 (Acute extensions of S)**.** Let $S \subset I^n$ be an acute 0/1-simplex with $k \le n$ vertices. The set $\mathcal{A}^n(S)$ of *acute extensions* of S consists of all $v \in \mathbb{B}^n$ such that $\operatorname{conv}(S, v)$ is an acute 0/1-simplex with $k+1$ vertices.

The following classical result formulates a necessary condition for a vertex $v \in \mathbb{B}^n$ of I^n to be an element of the set $\mathcal{A}^n(S)$ just defined.

Proposition 5.6 ([16])**.** *Let S be an acute n-simplex. Then each vertex of S projects orthogonally into the interior of its opposite $(n-1)$-dimensional facet.*

Definition 5.7 (Candidate acute extensions of S)**.** Let $S \subset I^n$ be an acute 0/1-simplex with $k \le n$ vertices. The set $\mathcal{C}^n(S)$ of *candidate acute extensions* of S consists of all $v \in \mathbb{B}^n$ such that v projects orthogonally into the interior of S.

Remark 5.8. Due to Proposition 5.6, we have that $\mathcal{A}^n(S) \subset \mathcal{C}^n(S)$. The sets are in general not equal. This can be seen in Figure 8. For each of the acute triangular facets $\mathcal{T}$ of the antipodal 0/1-tetrahedron in I^3, there exist *two* vertices of I^3 that project in the interior of $\mathcal{T}$, but only the convex hull of $\mathcal{T}$ with *one* of them yields an acute tetrahedron.

We will now investigate on a linear algebraic level when $v \in \mathcal{C}^n(S)$ or even $v \in \mathcal{A}^n(S)$. For this, let $P \in \mathbb{B}^{n\times k}$ with $1 \le k < n$ be such that $G = P^\top P$ satisfies the conditions (a) and (b) in Definition 5.1, and let $v \in \mathbb{B}^n$. Consider the matrix $[P|v]$. Its Gramian $\hat{G}$ is a simple update of G. Also its inverse $\hat{G}^{-1}$ is an update of the inverse H of G, as depicted in Figure 13. Note that $\hat{G}$ is positive semi-definite. It is invertible if and only if $s > 0$. This condition will turn out to be automatically fulfilled if v projects in the interior of its opposite facet.

Lemma 5.9. *The vertex v is an element of $\in \mathcal{C}^n(S)$ if and only if $h > 0$ and $e^\top h < 1$.*

Proof. Observe that the orthogonal projection of v on the column span of P equals Ph, because

$$Ph = P(P^\top P)^{-1}P^\top v \tag{55}$$

To lie in the *interior* of the corresponding facet of S, Ph must be a convex combination in which all vertices of that facet, including the origin, participate nontrivially. Thus, the entries of h must be positive and up to less than one. □

Corollary 5.10. *If $h > 0$ and $e^\top h < 1$ then $s > 0$.*

Proof. If v projects in the interior of its opposite facet, then in particular, v is not equal to a vertex of that facet. Also, no vertex of I^n is a convex combination of any of the others. Thus, the convex hull of the facet and v has nonzero volume. □

The diagram in Figure 13 and Lemma 5.9 again show that even if $v \in \mathcal{C}^n(S)$, it does not need to be in $\mathcal{A}^n(S)$. Indeed, because $hsh^\top > 0$, the updated matrix $H + hsh^\top$ may have nonnegative off-diagonal entries and violate condition (a) in Definition 5.1. Moreover, condition (b) may also be violated, as the row sums of $\hat{G}^{-1}$ equal

$$\begin{bmatrix} r \\ \rho \end{bmatrix} = \hat{G}^{-1}\begin{bmatrix} e \\ 1 \end{bmatrix} = \begin{bmatrix} He + sh(h^\top e - 1) \\ s(1 - h^\top e) \end{bmatrix} \tag{56}$$

and if $v \in \mathcal{C}^n(S)$ then according to Lemma 5.9, $h^\top e - 1 < 0$. Although this implies that $\rho > 0$, some of the remaining entries of r may be negative, in spite of $He > 0$.

Suppose now that $[P|v]$ is indeed such, that $v \in \mathcal{C}^n(S)$ but that $v/\in \mathcal{A}^n(S)$. For some $w \in \mathbb{B}^m$, consider the matrix

$$\left[\begin{array}{c|c} P & v \\ \hline 0 & w \end{array}\right] \quad \text{with Gramian} \quad \tilde{G} = \left[\begin{array}{c|c} P^\top P & P^\top v \\ \hline v^\top P & v^\top v + w^\top w \end{array}\right]$$

In comparison with the Gramian $\hat{G}$ in Figure 13, only the bottom right entry has changed. Obviously, it $w^\top w$ is large enough, the corresponding value of s will decrease so much, that the off-diagonal entries of $H + hsh^\top$ are negative, and the row sums in (56) positive.

In other words, if a vertex v projects in the interior of an acute facet F, then by moving v orthogonally away from F, the simplex conv(F, v) will ultimately always become acute.

The above discussion proves the following theorem.

Theorem 5.11. *Let S be an acute $0/1$-simplex in I^n. Consider I^n as a facet of I^{n+m}. Let the first n entries of $v \in \mathbb{B}^{n+m}$ correspond to the vertices of I^n. Then:*

$$\mathcal{C}^{n+m}(S) = \left\{ \begin{bmatrix} v \\ w \end{bmatrix} \quad | \quad v \in \mathcal{C}^n(S), \quad w \in \mathbb{B}^m \right\}. \tag{57}$$

and

$$\mathcal{A}^{n+m}(S) \supset \left\{ \begin{bmatrix} v \\ w \end{bmatrix} \quad | \quad v \in \mathcal{A}^n(S), \quad w \in \mathbb{B}^m \right\}. \tag{58}$$

Moreover, for each $v \in \mathcal{C}^n(S)$ there exists an ℓ such that

$$w^\top w \geq \ell \quad \Leftrightarrow \quad \begin{bmatrix} v \\ w \end{bmatrix} \in \mathcal{A}^{n+m}(S) \tag{59}$$

provided that m is large enough.

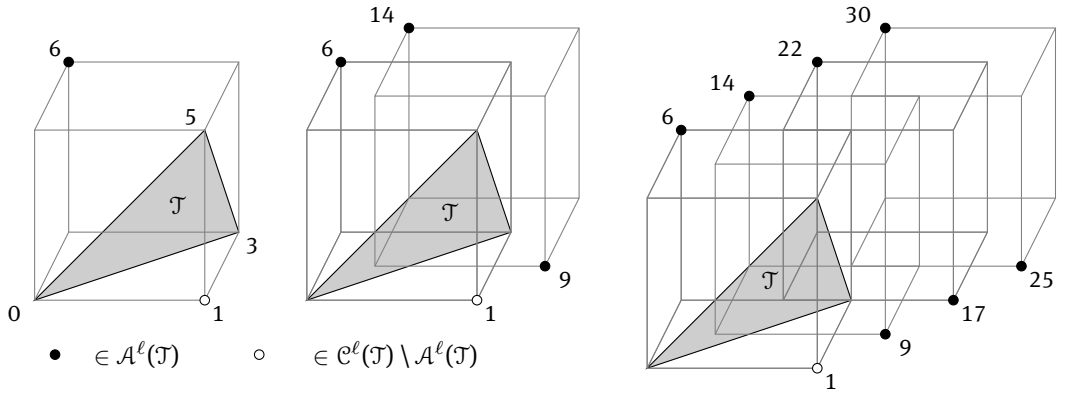

Figure 14: Impression of the structure of the sets $\mathcal{A}^\ell(\mathcal{T})$ and $\mathcal{C}^\ell(\mathcal{T})$ for increasing values of ℓ. The white vertex is not in $\mathcal{A}^\ell(\mathcal{T})$ but the ones "orthogonally above" it, are in $\mathcal{A}^\ell(\mathcal{T})$.

Proof. Statement (57) follows because the right-hand side consists precisely of those vertices of I^{n+m} whose orthogonal projection on I^n land in $\mathcal{C}^n(S)$. The claims in (58) and (59) follow from the above discussion. □

Note that the optimal value of ℓ in (59) can, in principle, be computed as soon as the data H, h, g and γ are available, as is visible from Figure 13.

Figure 14 serves to illustrate the claims of Theorem 5.11. Consider the acute 0/1-triangle $\mathcal{T}$ with vertices 0, 3, 5, in the numbering of Figure 5. The set $\mathcal{C}^3(\mathcal{T})$ consists of vertices 1 and 6, as both project in the interior of $\mathcal{T}$. Only vertex 6 is an element of $\mathcal{A}^3(\mathcal{T})$. Indeed, the tetrahedron formed by 1 and $\mathcal{T}$ is not acute: it has *right* dihedral angles. However, each of the vertices 9, 17, 25 *orthogonally above* vertex 1 forms an acute 0/1-tetrahedron with $\mathcal{T}$ and thus belong to $\mathcal{A}^5(\mathcal{T})$, as do the ones 14, 22, 30 orthogonally above vertex 6. The value of Theorem 5.11 is that in order to determine the set $\mathcal{A}^n(S)$ of a given minimal representative of an acute 0/1-simplex S, the computational work can be reduced to:

- find the smallest $k \le n$ for which $S \in I^k$ and determine $\mathcal{C}^k(S)$;
- determine which $v \in \mathcal{C}^k(S)$ are in $\mathcal{A}^k(S)$;
- for each $v \in \mathcal{C}^k(S) \setminus \mathcal{A}^k(S)$, determine the value of ℓ in (59).

After doing so, all remaining vertices of $v \in \mathbb{B}^n$ that are in $\mathcal{A}^n(S)$ can now be easily listed without having to verify acuteness of the simplex $\mathrm{conv}(S, v)$.

The next theorem is not difficult, but will play a central role in the enumeration problem.

Theorem 5.12. *Let $S \subset I^n$ be an acute 0/1-simplex with k vertices. If $\hat{S}$ is an acute 0/1-simplex in I^n having S as a facet, then each vertex of $\hat{S}$ belongs to S or to $\mathcal{A}^n(S)$.*

Proof. Let v be a vertex of $\hat{S}$ that does not belong to S. Then $\mathrm{conv}(S, v)$ is a facet of $\hat{S}$. Since $\hat{S}$ is acute, Proposition 5.3 shows that $\mathrm{conv}(S, v)$ is acute, and thus $v \in \mathcal{A}^n(S)$. □

In the language of Figure 14, Theorem 5.12 expresses that each acute 0/1-simplex having $\mathcal{T}$ as a triangular facet, has all its vertices amongst the black bullets. Note that for each of these black bullets, its projection on the triangle $\mathcal{T}$ is the orthocenter of $\mathcal{T}$.

Corollary 5.13. *Let $\mathcal{T}$ be a facet of an acute 0/1-simplex S. Then $\mathcal{A}^n(S) \subset \mathcal{A}^n(\mathcal{T})$.*

Theorem 5.12 shows the importance of administrating the set of acute extensions in the process of building acute 0/1-simplices from the starting point of a minimal representative an acute 0/1-triangle $\mathcal{T}$. Adding vertices to $\mathcal{T}$, the set of acute extensions of the resulting simplices becomes smaller and smaller as the dimension

of the simplex become larger, hence reducing the amount of work to be done to build all minimal representatives of 0/1-simplices having $\mathcal{T}$ as minimal triangular facet.

It remains necessary to work with the concept of minimal matrix representations, to reduce the amount of data to be computed. Not only *after* the construction process but also *during*.

5.2 Minimal acute extensions of acute 0/1-simplices

Let $\mathcal{T}^\star$ be a minimal representative of an acute 0/1-triangle in I^n with minimal matrix representation $T^\star$. Thus, the vertices of $\mathcal{T}^\star$ are the column vectors of $T^\star$. Now, consider the p matrices of size $n \times 4$ defined by

$$[T^\star|t_1], \quad \dots \quad , \quad [T^\star|t_p], \tag{60}$$

where $\mathcal{A}^n(\mathcal{T}^\star) = \{t_1, \dots, t_p\}$ is the set of acute extensions of $\mathcal{T}^\star$.

Proposition 5.14. *Each minimal matrix representation of each acute* 0/1*-tetrahedron having* $\mathcal{T}^\star$ *as minimal triangular facet, is among the matrices in (60).*

Proof. This follows immediately from Corollary 5.4 and the fact that there are no other $t \in I^n$ such that $[T^\star|t]$ is an acute 0/1-tetrahedron. □

Consequently, we can subdivide the set of acute extensions of a minimal representative of an acute 0/1-simplex into a minimal and a non-minimal part.

Definition 5.15 (Minimal acute extensions)**.** The set $\mathcal{A}^n(\mathcal{T}^\star)$ of acute extensions of a minimal representative $\mathcal{T}^\star$ of an acute 0/1-simplex with $k \le n$ vertices, with minimal matrix representation $T^\star$, is subdivided as

$$\mathcal{A}^n_\star(\mathcal{T}^\star) = \{t \in \mathcal{A}^n(\mathcal{T}^\star) \quad | \quad [T^\star|t] \quad \text{is a minimal matrix representation}\}$$

and its complement $\mathcal{A}^n_\circ(\mathcal{T}^\star)$ in $\mathcal{A}^n(\mathcal{T}^\star)$.

The results of Section 4 immediately show that the following matrices in (60) are in $\mathcal{A}^n_\circ(\mathcal{T}^\star)$:

(i) the ones for which the *column number* $v_n^\top t_j$ of t_j is *smaller* than $v_n^\top T^\star e_3$;

(ii) the ones for which the *row numbers* $[T^\star|t_j]w_4$ are *not* non-increasing.

To make the subdivision of $\mathcal{A}^n(\mathcal{T}^\star)$ in (60) into $\mathcal{A}^n_\star(\mathcal{T}^\star)$ and $\mathcal{A}^n_\circ(\mathcal{T}^\star)$ complete, one may use an adapted version of Algorithm 3; adapted in the sense that it should be aborted as soon as a matrix representation is encountered that proves that $[T^\star|t_j]$ is not minimal.

Remark 5.16. Note that if

$$[T^\star|t_j] = \left[\begin{array}{c|c} T^\star & t_j^1 \\ \hline 0 & t_j^2 \end{array}\right] \quad \text{with} \quad t_j^2 \in \mathbb{B}^m,$$

then $[T^\star|t_j]w_4$ is not non-increasing if t_j^2 itself is not non-increasing. Thus, for a number of $t \in \mathcal{A}^n(\mathcal{T}^\star)$ it may be directly indicated that they do not belong to $t \in \mathcal{A}^n_\star(\mathcal{T}^\star)$.

Suppose that it has been established that the matrix $[T^\star|t_\ell]$ is a minimal matrix representation of a 0/1-tetrahedron with minimal representative $\hat{\mathcal{T}}^\star$. In order to continue the construction process of acute 0/1-simplices efficiently, either in a *depth-first* or a *breadth-first* fashion, the data structures of acute candidates and acute extensions of $\hat{\mathcal{T}}^\star$ need to be updated.

Remark 5.17. It may happen that while t is not a minimal acute extension of some acute 0/1-simplex $\mathcal{T}^\star$, it *is* indeed a minimal acute extension of an acute simplex having $\mathcal{T}^\star$ as minimal facet. Indeed, let

$$T^\star = \begin{bmatrix} 0 & 1 & 1 \\ 0 & 1 & 0 \\ 0 & 0 & 1 \\ 0 & 0 & 0 \\ 0 & 0 & 0 \end{bmatrix}, \quad t_1 = \begin{bmatrix} 1 \\ 0 \\ 0 \\ 1 \\ 0 \end{bmatrix} \quad \text{and} \quad t_2 = \begin{bmatrix} 1 \\ 0 \\ 0 \\ 0 \\ 1 \end{bmatrix}. \tag{61}$$

Then both t_1 and t_2 are acute extensions of $T^\star$. Only t_1 is a minimal acute extension of $T^\star$, whereas t_2 is not due to criterion (i) above. But t_2 is a minimal acute extension of the minimal matrix representation $[T^\star|t_1]$.

Due to Corollary 5.13 we have that $\mathcal{A}^n(\hat{\mathcal{T}}^\star) \subset \mathcal{A}^n(\mathcal{T}^\star)$. To determine $\mathcal{A}^n(\hat{\mathcal{T}}^\star)$ *exactly*, it may not be necessary to verify for *each* $t \in \mathcal{A}^n(\mathcal{T}^\star)$ whether the convex hull $\mathrm{conv}(\hat{\mathcal{T}}^\star, t)$ of $\hat{\mathcal{T}}^\star$ and t is an acute 0/1-simplex. Indeed, if $\hat{\mathcal{T}}^\star \subset I^k$ for some $k < n$, it suffices to find out which $t \in \mathcal{A}^k(\mathcal{T}^\star)$ are in $\mathcal{C}^k(\hat{\mathcal{T}}^\star)$ and which of these are in $\mathcal{A}^k(\hat{\mathcal{T}}^\star)$ and then use Theorem 5.11.

Example. The matrix $T^\star \in \mathbb{B}^{6\times 3}$ in (62) with vertex numbers 0, 3 and 13, is a minimal matrix representation of a minimal representative $\mathcal{T}^\star$ of an acute 0/1-triangle. Clearly $\mathcal{T}^\star \subset I^4$. The vertices from I^4 that are in $\mathcal{C}^4(\mathcal{T}^\star)$ are listed by their vertex numbers 1, 5, 6, 9, 10 and 12 as well as their 0/1-vectors. The numbers in the row indicated by $\mathcal{A}^4(\mathcal{T}^\star)$ correspond to the smallest value m of entries equal to one need to be appended to the vector above it such that it becomes an element of $\mathcal{A}^{n+m}(\mathcal{T}^\star)$.

$T^\star =$

0	1	1
0	1	0
0	0	1
0	0	1
0	0	0
0	0	0
0	3	13

$\mathcal{C}^4(\mathcal{T}^\star)$	1	5	6	9	10	14
	1	1	0	1	0	0
	0	0	1	0	1	1
	0	1	1	0	0	1
	0	0	0	1	1	1
$\mathcal{A}^4(\mathcal{T}^\star)$	1	1	0	1	0	0
$\mathcal{A}^5(\mathcal{T}^\star)$	17	21	22	25	26	30
$\mathcal{A}^6(\mathcal{T}^\star)$	33	37	38	41	42	46
	49	53	54	57	58	62

(62)

Thus, the vertices 6, 10 and 14 are in $\mathcal{A}^4(\mathcal{T}^\star)$, and the vertices 1, 5 and 9 are candidates that need only one additional 1 to become acute extensions. This is visible in the next row, where the vertex numbers of *additional* vertices in $\mathcal{A}^5(\mathcal{T}^\star)$ are displayed, which are the ones from $\mathcal{C}^4(\mathcal{T}^\star)$ plus $2^4 = 16$. Finally, the elements from $\mathcal{A}^6(\mathcal{T}^\star)$ *additional* to the ones from $\mathcal{A}^4(\mathcal{T}^\star)$ and $\mathcal{A}^5(\mathcal{T}^\star)$ are precisely those with $2^5 = 32$ added. It can easily be verified that only 14, 17, 21, 22, 30, 49, 53, 54, 62 remain after removing the ones that fall under the items (i) or (ii) below Definition 5.15. It is also not hard to see that the matrix $\hat{T}^\star$ with column numbers 0, 3, 13, 21 is indeed a minimal matrix representation of a 0/1-tetrahedron $\hat{\mathcal{T}}^\star \subset I^5$. To determine $\mathcal{A}^6(\hat{\mathcal{T}}^\star)$, we re-investigate the each of the vertices 1, 5, 6, 9, 10, 14, 17, 21, 22, 25, 26, 30 and indicate whether it belongs to $\mathcal{C}^5(\hat{\mathcal{T}}^\star)$ or $\mathcal{A}^5(\hat{\mathcal{T}}^\star)$ or neither. This determines which of the vertices in 33, 37, 38, 41, 42, 46, 49, 53, 54, 57, 58, 62 are *additionally* in $\mathcal{A}^6(\hat{\mathcal{T}}^\star)$.

6 A special class of acute 0/1-simplices

Here we analyze the computational results of the codes presented in Section A. Looking at the structure of the 0/1-matrices presented there, we observe some patterns. Although not all patters can be mathematically accounted for, there is one pattern that can be fully explained.

Remark 6.1. Since each first column of a minimal matrix representation is zero according to Corollary 4.11, we will omit this redundant column from the notation. What remains is a square matrix, whose Gramian has an inverse that is a diagonally dominant strictly Stieltjes matrix, and which we will also call a minimal matrix representation. See Definition 5.1.

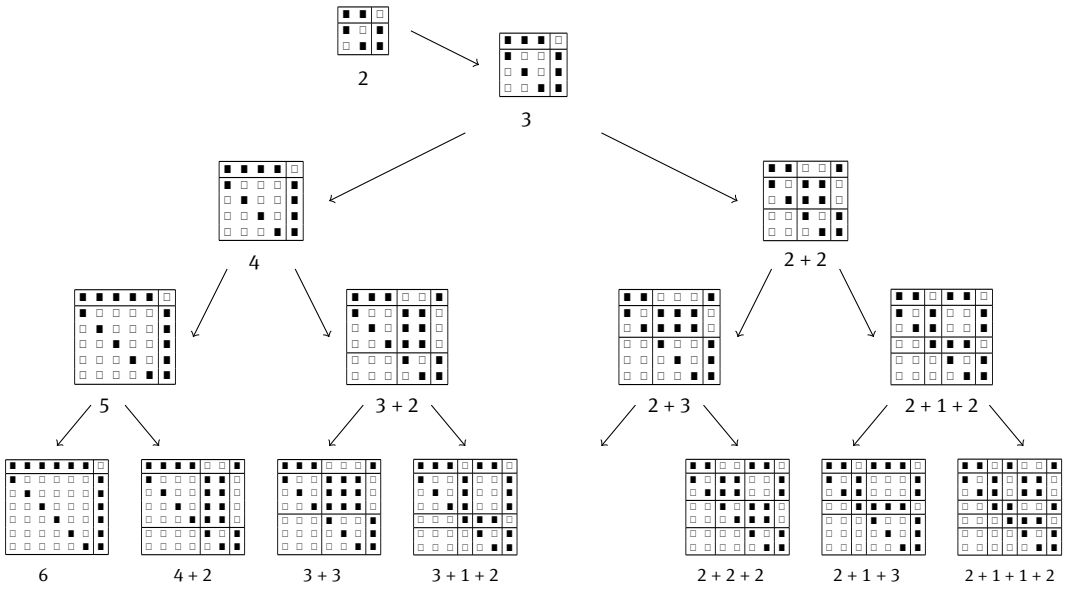

Figure 15: Upper Hessenberg matrix representations and integer compositions.

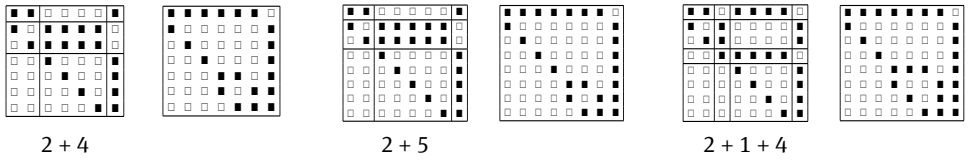

Figure 16: Upper Hessenberg matrices corresponding to integer compositions $2+4$, $2+5$, and $2+1+4$. Next to them are depicted the corresponding minimal matrix representations.

6.1 Acute simplices with upper Hessenberg matrix representations

The computational results in Section A show that all acute 0/1-simplices in I^3, I^4 and I^5 have a minimal matrix representation that is an *unreduced upper Hessenberg matrix*. For $n \geq 6$, many, but not all of them are unreduced upper Hessenberg. A closer inspection of these matrices shows that each of them corresponds to a unique *composition* of the integer $n-1$.

Definition 6.2 (Integer composition)**.** A *composition* of an integer n in k parts is an ordered k-tupel $\lambda = \langle \lambda_1, \ldots, \lambda_k \rangle$ with $\lambda_j \in \mathbb{N}$ with the property that $n = \lambda_1 + \lambda_2 + \cdots + \lambda_k$.

In Figure 15 we depict the observed correspondence, restricted to $n \leq 7$, as a binary tree. The first $n-1$ entries in the first row of each matrix form an integer composition $\langle \lambda_1, \ldots, \lambda_k \rangle$ of $n-1$, by considering consecutive entries with the *same value* as belonging to the *same part*. The last $n-1$ entries of the last column show the same composition. The horizontal and vertical lines separating the parts of both compositions, subdivide the matrix in blocks. There are *k identity matrices* of consecutive sizes $\lambda_1 \times \lambda_1, \ldots, \lambda_k \times \lambda_k$ containing the first sub-diagonal. The blocks above those identity matrices alternatingly contain only zeros or only ones, starting with ones directly above the identity matrices.

Remark 6.3. In Figure 15, the matrix corresponding to the composition $2+4$ of 6 is missing. This is because it is not a *minimal* matrix representation. The matrix that *is* a minimal matrix representation of the corresponding simplex is *not* upper Hessenberg. In Figure 16, it is depicted to its right. The same is done for the compositions $2+5$ and $2+1+4$ of 7.

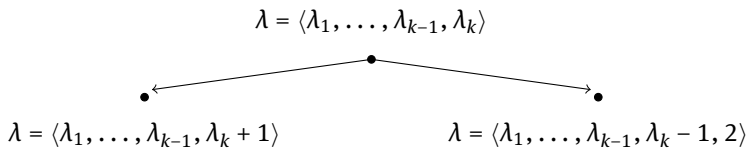

Figure 17: Splitting rule that defines the binary tree in Figure 15.

Proposition 6.4. *The matrix H_λ corresponding to an integer partition $\langle \lambda_1, \ldots, \lambda_k \rangle$ is not a minimal matrix representation if $\lambda_j > \lambda_1 + 1$ for some $j \in \{2, \ldots, k\}$.*

Proof. The first λ_1 columns of H_λ should, together with the origin, form the largest possible subset of vertices with mutual distances equal to two. If $\lambda_j > \lambda_1 + 1$, this is not the case. □

Now, let $n \geq 4$ be given, and let $\lambda = \langle \lambda_1, \ldots, \lambda_k \rangle$ be an integer composition of $n-1$ with the property that $\lambda_1 / = 1 / = \lambda_k$. It can easily be verified that there are 2^{n-4} such compositions.

We will write H_λ for the upper Hessenberg matrix that corresponds to λ according to the above description and examples. See also the introduction to this paper. The rule defining the tree in Figure 15 is now depicted in Figure 17. In the next section we will prove that for given n, each of the 2^{n-4} matrices H_λ corresponding to a composition λ of $n-1$ with first and last part at least 2, represents an acute 0/1-simplex. Conversely, we will show that if H is an $n \times n$ unreduced upper Hessenberg matrix that represents an acute 0/1-simplex, then $H \sim H_\lambda$ for some composition λ of $n-1$.

6.2 An application of the one neighbor theorem

We first recall the following theorem, which limits the number of candidate acute extensions from Definition 5.7 of an acute simplex in I^n with n vertices to two.

Theorem 6.5 ([4])**.** *Let F be an acute 0/1 simplex in I^n with n vertices. Then $\mathcal{C}^n(F) \subset \mathbb{B}^n$ consists of at most two points. If it consists of two points, they add up to $e = (1, \ldots, 1)^\top$.*

In the context of triangulations this result is called the *one neighbor theorem*, since it proves that an acute simplex in I^n has at most one face-to-face neighbor in I^n. See [4, 13] for applications of this result in nonobtuse triangulations of I^n, and of 0/1-polytopes in I^4, respectively. Here, we will apply the result to prove the observed structures in Section 6.1.

Lemma 6.6. *Let H be an $n \times (n-1)$ unreduced upper Hessenberg 0/1-matrix, whose columns together with the origin form an acute $(n-1)$-simplex in I^n. Then there exist at most two $(n+1) \times n$ unreduced upper Hessenberg matrices whose columns together with the origin form an acute n-simplex in I^{n+1}, that have H as top left $n \times (n-1)$ part.*

Proof. Let H be an $n \times (n-1)$ unreduced upper Hessenberg 0/1-matrix, whose columns together with the origin form an acute $(n-1)$-simplex. Then due to Theorem 6.5, there exists *at most* two vertices $g, h \in \mathbb{B}^n$ with $g + h = e$ such that the $n \times n$ matrices $[H|g]$ and $[H|h]$ represent acute n-simplices in I^n. As a result, only

$$\left[\begin{array}{c|c} H & g \\ \hline 0 & 1 \end{array}\right] \quad \text{and} \quad \left[\begin{array}{c|c} H & h \\ \hline 0 & 1 \end{array}\right] \tag{63}$$

may be $(n+1) \times n$ unreduced upper Hessenberg matrices whose columns together with the origin form acute n-simplices in I^{n+1}. □

Corollary 6.7. *There exist at most 2^{n-2} unreduced upper Hessenberg matrices of size $n\times(n-1)$ whose columns together with the origin are the vertices of an acute $(n-1)$-simplex.*

Proof. One can easily verify that in I^3, the matrices

$$H_1=\begin{bmatrix}1&1\\1&0\\0&1\end{bmatrix}\quad\text{and}\quad H_2=\begin{bmatrix}1&0\\1&1\\0&1\end{bmatrix}$$

are the only two 3×2 upper Hessenberg matrices whose columns together with the origin are acute triangles in I^3, the statement is now proved by induction based on Lemma 6.6. □

Since H_2 is obtained from H_1 by swapping its first two rows, we see that any unreduced upper Hessenberg matrix that is a *minimal* matrix representation, has H_1 as its top 3×2 block.

Corollary 6.8. *The only two $(n+1)\times(n+1)$ unreduced upper Hessenberg matrices with $n\times(n-1)$ top left part equal to H that may represent acute $(n+1)$-simplices are*

$$\left[\begin{array}{c|c|c}H&g&h\\\hline 0&1&1\end{array}\right]\quad\text{and}\quad\left[\begin{array}{c|c|c}H&h&g\\\hline 0&1&1\end{array}\right].\tag{64}$$

In case they do, these two matrices obviously represent the same $0/1$-simplex, and thus at most one of them can be a minimal matrix representation.

Proof. Suppose that both $(n+1)\times n$ matrices in (63) indeed represent acute n-simplices in I^{n+1}. Suppose moreover that adding $v\in\mathbb{B}^{n+1}$ as a $(n+1)$-st column results in a matrix representing an acute $(n+1)$-simplex. Then due to Theorem 6.5, the top n entries of v should consist of g or h. For the left matrix in (63) this leads to four options,

$$\left[\begin{array}{c|c|c}H&g&g\\\hline 0&1&0\end{array}\right],\quad\left[\begin{array}{c|c|c}H&g&g\\\hline 0&1&1\end{array}\right],\quad\left[\begin{array}{c|c|c}H&g&h\\\hline 0&1&0\end{array}\right]\quad\text{and}\quad\left[\begin{array}{c|c|c}H&g&h\\\hline 0&1&1\end{array}\right].\tag{65}$$

We claim that only the rightmost matrix in (65) may represent an acute $(n+1)$-simplex. Indeed, the difference between the last two columns of the first matrix is orthogonal to the last. Thus, it has a right triangular facet, and thus due to Proposition 5.3 it cannot represent an acute simplex. The second matrix is obviously singular. The last two columns of the third matrix are orthogonal because $g+h=e$ and thus this simplex too has a right triangular facet. Thus, the fourth matrix remains. For the right matrix in (63) a similar analysis can be made. Finally, note that the matrices in (64) differ only by swapping the last columns. □

To be able to fully explain the tree in Figure 15, we will need to go one step further, and even describe which $(n+2)\times(n+2)$ unreduced upper Hessenberg matrices with $n\times(n-1)$ part equal to H have the potential to be a minimal matrix representation of an acute $(n+2)$-simplex.

Corollary 6.9. *Assume that the right matrix in (64) is not a minimal matrix representation. Then*

$$\left[\begin{array}{c|c|c|c}H&g&g&h\\\hline 0&1&0&1\\\hline 0&0&1&1\end{array}\right]\quad\text{and}\quad\left[\begin{array}{c|c|c|c}H&h&h&g\\\hline 0&1&0&1\\\hline 0&0&1&1\end{array}\right]\tag{66}$$

are the only two $(n+2)\times(n+2)$ unreduced upper Hessenberg matrices with the $n\times(n-1)$ unreduced upper Hessenberg matrix H as top left part, that may be minimal matrix representations of an acute $(n+2)$-simplex.

Proof. We follow the lines of the proofs of Lemma 6.6 and Corollary 6.8 but then with H consecutively replaced by each of the two matrices in (63). Consider first the left matrix in (63). It gives rise to the following four

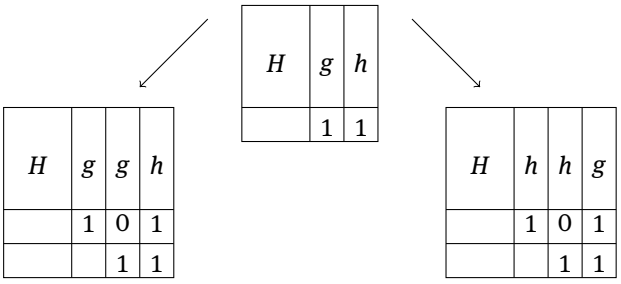

Figure 18: Splitting rule that defines the binary tree in Figure 15, in matrix form.

candidates,

$$\left[\begin{array}{c|c|c} H & g & v \\ \hline 0 & 1 & a \\ \hline 0 & 0 & 1 \end{array}\right] \quad \text{with} \quad v \in \{g, h\} \quad \text{and} \quad a \in \{0, 1\}. \tag{67}$$

The option $(v, a) = (g, 1)$ and $(v, a) = (h, 0)$ both lead to a right triangular facet and are thus infeasible. The remaining options are $(v, a) = (g, 0)$ and $(v, a) = (h, 1)$, which, in line with the proof of Lemma 6.6, add up to the all-ones vector. Moreover, in line with Corollary 6.8, they account for the left matrix in (66). For the right matrix in (63), conversely, only the options $(v, a) = (h, 0)$ and $(v, a) = (g, 1)$ are feasible, and lead to the right matrix in (66). □

Corollary 6.9 explicitly proves that an unreduced upper Hessenberg matrix H_λ of size $(n+1) \times (n+1)$ that represents an acute simplex, can have at most two unreduced upper Hessenberg descendants of size $(n+2) \times (n+2)$ that represent an acute simplex, and who share their $n \times (n-1)$ top left parts. This is depicted in Figure 18. This also proves that for each unreduced upper Hessenberg matrix that represents an acute 0/1-simplex, there exists a matrix H_λ in the tree in Figure 15 with which it is 0/1-equivalent.

We will now proceed to prove that each of the 2^{n-4} unreduced upper Hessenberg matrices in the tree indeed represents an acute simplex. For this, we will use the concept of strictly ultrametric matrix, as defined in Section 1.1.

Theorem 6.10. *Let H_λ be the unreduced upper Hessenberg matrix corresponding to the integer decomposition $\lambda = \langle \lambda_1, \ldots, \lambda_k \rangle$ of $n-1$. Then $G_\lambda = H_\lambda^\top H_\lambda$ is strictly ultrametric.*

Proof. We use the splitting rule proved in Corollaries 6.8 and 6.9 and depicted in Figure 14 as starting point for an inductive proof. Consider the $n+1$ columns of the parent matrix in Figure 14, and write them as

$$\left[\begin{array}{c} h_1 \\ \hline 0 \end{array}\right], \ldots, \left[\begin{array}{c} h_{n-1} \\ \hline 0 \end{array}\right], \quad \left[\begin{array}{c} g \\ \hline 1 \end{array}\right] \quad \text{and} \quad \left[\begin{array}{c} h \\ \hline 1 \end{array}\right]. \tag{68}$$

By definition of strict ultrametricity, there is no triple u, v, w of distinct columns taken from (68) such that one of the three numbers $u^\top v, v^\top w, w^\top u$ is smaller than the other two. We will prove this property also for the $n+2$ columns of the left descendant in Figure 14, which are

$$\left[\begin{array}{c} h_1 \\ \hline 0 \\ 0 \end{array}\right], \ldots, \left[\begin{array}{c} h_{n-1} \\ \hline 0 \\ 0 \end{array}\right], \quad \left[\begin{array}{c} g \\ \hline 1 \\ 0 \end{array}\right], \quad \left[\begin{array}{c} h \\ \hline 1 \\ 1 \end{array}\right] \quad \text{and the new column} \quad \left[\begin{array}{c} g \\ \hline 0 \\ 1 \end{array}\right]. \tag{69}$$

Obviously, each triple taken from (69) that does not contain the new column has the same mutual inner products as a triple from (68). The same clearly holds for each of the triples

$$\left\{ \left[\begin{array}{c} h_i \\ \hline 0 \\ 0 \end{array}\right], \left[\begin{array}{c} h_j \\ \hline 0 \\ 0 \end{array}\right], \left[\begin{array}{c} g \\ \hline 0 \\ 1 \end{array}\right] \right\} \quad \text{and} \quad \left\{ \left[\begin{array}{c} h_i \\ \hline 0 \\ 0 \end{array}\right], \left[\begin{array}{c} h \\ \hline 1 \\ 1 \end{array}\right], \left[\begin{array}{c} g \\ \hline 0 \\ 1 \end{array}\right] \right\}.$$

Two possible triples remain to be discussed, being

$$\left\{ \left[\begin{array}{c} h_i \\ \hline 0 \\ 0 \end{array}\right], \left[\begin{array}{c} g \\ \hline 1 \\ 0 \end{array}\right], \left[\begin{array}{c} g \\ \hline 0 \\ 1 \end{array}\right] \right\} \quad \text{and} \quad \left\{ \left[\begin{array}{c} g \\ \hline 1 \\ 0 \end{array}\right], \left[\begin{array}{c} h \\ \hline 1 \\ 1 \end{array}\right], \left[\begin{array}{c} g \\ \hline 0 \\ 1 \end{array}\right] \right\}.$$

For the left triple, we use the generally valid fact that $x^\top y \le x^\top x$ for all $x, y \in \mathbb{B}^n$ to conclude that $h_j^\top g \le g^\top g$, which proves the required property. For the right triple it suffices to note that $g^\top h = 0$ and $g^\top g \ge 1$. Next, we consider the right descendant in Figure 14, with columns

$$\left[\begin{array}{c} h_1 \\ \hline 0 \\ 0 \end{array}\right], \ldots, \left[\begin{array}{c} h_{n-1} \\ \hline 0 \\ 0 \end{array}\right], \left[\begin{array}{c} h \\ \hline 1 \\ 0 \end{array}\right], \left[\begin{array}{c} g \\ \hline 1 \\ 1 \end{array}\right] \quad \text{and the new column} \quad \left[\begin{array}{c} h \\ \hline 0 \\ 1 \end{array}\right]. \tag{70}$$

Compared to (69), only the roles of g and h have been exchanged. This does not affect the validity of the above arguments. And thus both descendents are strictly ultrametric. Since the 3×3 matrix H_λ with $\lambda = \langle 2 \rangle$ has a strictly ultrametric Gramian, this proves the statement for all members H_λ of the tree in Figure 15 by induction. □

6.3 The absolute determinant of H_λ as continued fraction numerator

We are now able to derive an explicit expression for the determinant of H_λ for any given integer composition λ. For this, we associate with the parent matrix in Figure 18 two integers:

$$H_\lambda = \left[\begin{array}{c|c|c} H & g & h \\ \hline 0 & 1 & 1 \end{array}\right] \to \left[\begin{array}{c} p \\ q \end{array}\right] = \left[\begin{array}{c} \det(H|g) \\ \det(H|h) \end{array}\right]. \tag{71}$$

By developing the last row of H_λ, we have that $\det(H_\lambda) = p - q$, whereas for the descendants H_λ^ℓ and H_λ^r of H_λ, also by development of their last rows, we find that

$$\left[\begin{array}{c|c|c|c} H & g & g & h \\ \hline 0 & 1 & 0 & 1 \\ \hline 0 & 0 & 1 & 1 \end{array}\right] \to \left[\begin{array}{c} -p \\ p-q \end{array}\right] \quad \text{and} \quad \left[\begin{array}{c|c|c|c} H & h & h & g \\ \hline 0 & 1 & 0 & 1 \\ \hline 0 & 0 & 1 & 1 \end{array}\right] \to \left[\begin{array}{c} -q \\ q-p \end{array}\right]. \tag{72}$$

Since $p = 1$ and $q = -2$ for the matrix H_λ with $\lambda = \langle 3 \rangle$ at the root of the tree in Figure 11, we see that this explains the correspondence between the absolute determinants of the matrices H_λ and Kepler's Tree of Fractions, as claimed in Section 1.2. To additionally prove the statement in Theorem 1.2 that $\det(H_\lambda)$ equals the numerator f_k of the continued fraction

$$[\lambda_1; \lambda_2, \ldots, \lambda_k] = \lambda_1 + \cfrac{1}{\lambda_2 + \cfrac{1}{\ddots + \cfrac{1}{\lambda_k}}} = \frac{f_k}{g_k} \quad \text{with } f_k, g_k \text{ coprime} \tag{73}$$

we use the well-known result from continued fraction theory that f_k can be computed from the two-term recursion

$$f_j = \lambda_j f_{j-1} + f_{j-2}, \quad \text{with} \quad f_0 = 1 \quad \text{and} \quad f_{-1} = 0. \tag{74}$$

We inductively assume that the statement holds for both the parent and the grandparent of a vertex in the tree, and prove the statement for the descendants, as depicted in Figure 19. First observe that all seven continued fractions in Figure 19 start with the same $k - 1$ numbers $\lambda_1, \ldots, \lambda_{k-1}$. Denote the numerator of $[\lambda_1; \lambda_2, \ldots, \lambda_{k-2}]$ by f_{k-2} and the numerator of $[\lambda_1; \lambda_2, \ldots, \lambda_{k-1}]$ by f_{k-1}. Then the induction hypothesis on the grand parent in Figure 14 together with (74) imply that

$$p + q = \lambda_k f_{k-1} + f_{k-2},$$

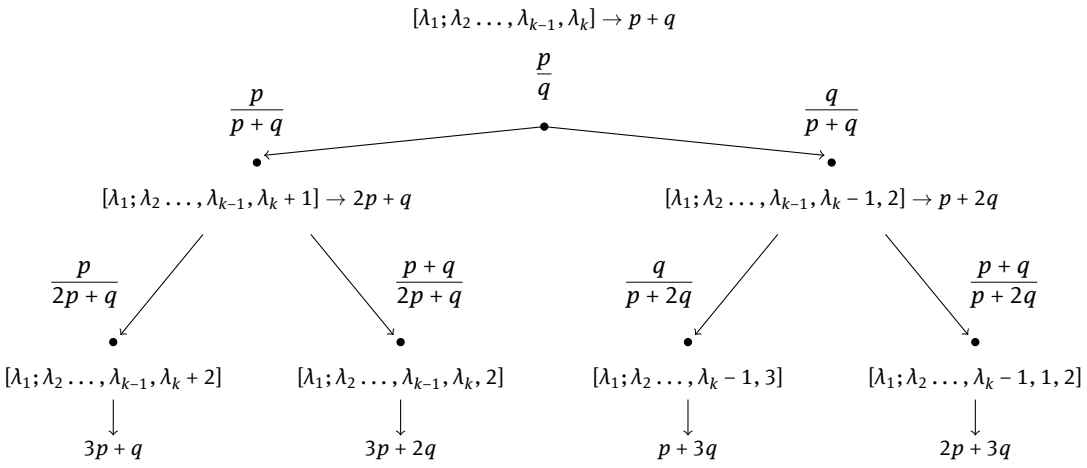

Figure 19: If parent and grandparent satisfy the statement, then so do the four descendants.

whereas the induction hypothesis on its left descendant translates to

$$2p+q=(\lambda_k+1)f_{k-1}+f_{k-2}.$$

From thes two relations we can solve f_{k-1} and f_{k-2} as

$$f_{k-1}=p \quad \text{and} \quad f_{k-2}=(1-\lambda_k)p+q.$$

It remains to verify whether these values for f_{k-1} and f_{k-2} are consistent with the remaining five continued fractions in Figure 14 and the expressions of their numerators in terms of p and q. First, for the continued fraction $[\lambda_1;\lambda_2,\ldots,\lambda_k-1,2]$ we find, taking two steps of (74) that its numerator indeed equals

$$2\cdot\left[(\lambda_k-1)f_{k-1}+f_{k-2}\right]+f_{k-1}=2\cdot\left[(\lambda_k-1)p+(1-\lambda_k)p+q\right]+p=p+2q.$$

Thus, if a vertex and its left descendant satisfy the statement, then so does its right descendant. Consequently, the only two continued fractions to verify are the two left descendants at the lowest level in Figure 19. For the continued fraction $[\lambda_1;\lambda_2,\ldots,\lambda_k+2]$ we find

$$(\lambda_k+2)f_{k-1}+f_{k-2}=(\lambda_k+2)p+(1-\lambda_k)p+q=3p+q$$

and for $[\lambda_1;\lambda_2,\ldots,\lambda_k-1,3]$

$$3\cdot[(\lambda_k-1)f_{k-1}+f_{k-2}]+f_{k-1}=3\cdot[(\lambda_k-1)p+(1-\lambda_k)p+q]+p=p+3q.$$

Since both are consistent, this finishes the induction step. As the induction basis for the first two levels of the tree in Figure 15 is easily verified, this completes the induction proof.

Acknowledgement: Jan Brandts and Apo Cihangir acknowledge the support by Research Project 613.001.019 of the Netherlands Organisation for Scientific Research (NWO), and are grateful to Michal Křížek for comments and discussions on earlier versions of the manuscript.

A Appendix: Computational results

In this final section of this paper we present a selection of the computational data obtained by implementations of the algorithms presented. For simplicity, we chose Matlab as programming environment, as Matlab contains useful built-in functionalities in the area of linear algebra. Faster imlementations can of course be obtained using a lower level programming language.

Table 10: The cycle indices Z_3, Z_4, Z_5, Z_6 and Z_7 in condensed tabulated form.

$\mathcal{B}_3$	1	2	3	4	6
12				2	
8		1			1
13		4			
8	2		2		
6	4	2			
1	8				

$\mathcal{B}_4$	1	2	3	4	6	8
48						2
84				4		
96		2			2	
51		8				
48	2	1		3		
32	4		4			
12	4	6				
12	8	4				
1	16					

$\mathcal{B}_5$	1	2	3	4	5	6	8	10	12
480							4		
320				2					2
520				8					
384		1						3	
720		4				4			
240		4		6					
231		16							
384	2				6				
240	4	2		6					
160	4	2	4			2			
80	8		8						
60	8	12							
20	16	8							
1	32								

$\mathcal{B}_7$	1	2	3	4	5	6	7	8	10	12	14	20	24
26880								4					4
53760								16					
32256				2								6	
53760				2						10			
47040				8						8			
43344				32									
46080		1									9		
72576		4							12				
58240		4				20							
13440		4		6		4				6			
35560		16				16							
21840		16		24									
5209		64											
46080	2						18						
16128	4	2			12				6				
26880	4	2	4			18							
13440	4	2	4	6		2				6			
8064	8				24								
4480	8		40										
10080	8	12		24									
3360	8	12	8			12							
1680	16	8		24									
3360	16	8	16			8							
840	16	56											
280	32		32										
420	32	48											
42	64	32											
1	128												

$\mathcal{B}_6$	1	2	3	4	5	6	8	10	12
5760							8		
3840				1					5
3840				4					4
4920				16					
6912		2						6	
1920		2				10			
5280		8				8			
2160		8		12					
1053		32							
3840	2	1	2			9			
2304	4				12				
640	4		20						
1440	4	6		12					
720	8	4		12					
960	8	4	8			4			
120	8	28							
160	16		16						
180	16	24							
30	32	16							
1	64								

A.1 The cycle index Z_n of $\mathcal{B}_n$ for the values $n \in \{3, \ldots, 9\}$

In Algorithm 1 in Section 2, we described how to compute the cycle index Z_n for the induced permutations of $\mathbb{B}^n$ by the hyperoctahedral group $\mathcal{B}_n$. The implementation of this algorithm yields each cycle index Z_n as a table. This table is a condensed form of the table in (4), in the sense that zero columns have been removed, and zero entries disregarded.

To generate partitions needed in Algorithm 1, we used Algorithm P in [25]. We also used the most efficient way to determine the cycle type of a given permutation, which is $\mathcal{O}(p)$ for a permutation of p objects. If $n \geq 10$ then all cycle type computations take more than ninety percent of the total computational time in computing Z_n, and this percentage increases for increasing n. Thus, no additional improvements of the algorithm can be expected.

Table 11: The cycle index Z_8 in condensed tabulated form.

$\mathcal{B}_8$	1	2	3	4	5	6	7	8	10	12	14	15	16	20	24	30
645120													16			
430080								8							8	
779520								32								
516096				4										12		
1218560				4						20						
465920				16						16						
445424				64												
1105920		2									18					
516096		2				2			6							6
709632		8							24							
698880		8				40										
322560		8		12		8				12						
243264		32				32										
171360		32		48												
26463		128														
645120	2	1		3				30								
368640	4						36									
172032	4		4		12							12				
80640	4	6		60												
215040	4	6	4			38										
129024	8	4			24				12							
107520	8	4	8			36										
107520	8	4	8	12		4				12						
35840	8	4	40			20										
40320	8	28		48												
21504	16				48											
17920	16		80													
40320	16	24		48												
26880	16	24	16			24										
1680	16	120														
3360	32	16		48												
8960	32	16	32			16										
3360	32	112														
448	64		64													
840	64	96														
56	128	64														
1	256															

Table 12: The cycle index Z_9 in condensed tabulated form.

$\mathcal{B}_9$	1	2	3	4	5	6	7	8	9	10	12	14	15	16	18	20	24	28	30	40
11612160														32						
4644864								4												12
7741440								16									16			
9386496								64												
6635520				2														18		
5160960				2							42									
8128512				8												24				
16773120				8							40									
6612480				32							32									
4317408				128																
10321920		1				1									28					
14929920		4										36								
10838016		4				4				12									12	
3584000		4				84														
2322432		4		6						12						18				
5806080		4		6				60												
6144768		16								48										
8117760		16				80														
4354560		16		24		16					24									
725760		16		120																
1637664		64				64														
1397088		64		96																
142207		256																		
10321920	2		2						56											
3317760	4	2					36					18								
5806080	4	2		6				60												
2322432	4	2		6	12					6						18				
2580480	4	2	20			74														
1658880	8						72													
1548288	8		8		24								24							
143360	8		168																	
580608	8	12			24					36										
725760	8	12		120																
1935360	8	12	8			76														
967680	8	12	8	24		12					24									
580608	16	8			48					24										
322560	16	8	16			72														
483840	16	8	16	24		8					24									
322560	16	8	80			40														
362880	16	56		96																
80640	16	56	16			56														
48384	32				96															
53760	32		160																	
120960	32	48		96																
120960	32	48	32			48														
15120	32	240																		
6048	64	32		96																
20160	64	32	64			32														
10080	64	224																		
672	128		128																	
1512	128	192																		
72	256	128																		
1	512																			

Table 13: Number of 0/1-polytopes in I^n with $0 \le k \le 2^n$ vertices for $n \le 5$.

$n\backslash k$	0	1	2	3	4	5	6	7	8	9	10	11	12	13	14	15	16
1	1	1	1														
2	1	1	2	1	1												
3	1	1	3	3	6	3	3	1	1								
4	1	1	4	6	19	27	50	56	74	56	50	27	19	6	4	1	1
5	1	1	5	10	47	131	472	1326	3779	9013	19963	38073	65664	98804	133576	158658	169112

Table 14: Number of 0/1-simplices in I^n with $1 \le k \le n+1$ vertices for $n \le 8$.

$n\backslash k$	1	2	3	4	5	6	7	8	9
1	1	1							
2	1	2	1						
3	1	3	3	6					
4	1	4	6	19	27				
5	1	5	10	47	131	472			
6	1	6	16	103	497	3253	19735		
7	1	7	23	203	1606	18435	221778	2773763	
8	1	8	32	373	4647	91028	2074059	51107344	1245930065

A.2 The number of 0/1-polytopes with *k* vertices

Using Algorithm 2 from Section 3, we computed the number of 0/1-polytopes with k vertices for $0 \le k \le 2^n$, for the values $n \le 5$. They are displayed in Table 13. For $n = 5$, only half of the results are displayed, as the results for $k = \ell$ and $k = 2^n - \ell$ are the same.

In Table 14, we zoom in on the 0/1-simplices in I^n with $k \le n+1$ vertices. In Table 15 we present the number of ways to choose k points from $\mathbb{B}^n$. Comparing these numbers with the corresponding numbers in Table 14 shows the large gain of working modulo the action of $\mathcal{B}_n$.

Remark A.1. Note that for $k \ge 4$ these numbers include *degenerate* k-simplices, which lie in a hyperplane of dimension less than k. For $k \in \{2, 3\}$ such degenerate cases do not exist: three distinct point in I^n are never colinear.

Finally, in Table 16 we compare the number $a(n)$ of *acute* 0/1-simplices in I^n with their *total* number $s(n)$, both modulo the action of $\mathcal{B}_n$.

A.3 Minimal matrix representations of acute 0/1-simplices

Here we present the computed minimal matrix representations (without their zero first column) of all acute 0/1-simplices with $n+1$ vertices in I^n for $3 \le n \le 9$ together with the absolute values of their determinants.

Table 15: Binomial coefficients $\binom{2^n}{k}$ for comparison with Table 2.2.

$n\backslash k$	1	2	3	4	5	6	7
1	2	1					
2	4	6	4				
3	8	28	56	70			
4	16	120	560	1820	4368		
5	32	496	4960	35960	201376	906192	
6	64	2016	41664	635376	7624512	74974368	621216192

Table 16: The number $a(n)$ of *acute* $0/1$ n-simplices related to their *total* number $s(n)$.

n	1	2	3	4	5	6	7	8	9	10	11
$a(n)$	1	0	1	1	2	6	13	29	67	162	392
$s(n)$	1	1	6	27	472	19735	2773763	1245930065	$1.8e12$	$8.7e15$	$1.3e20$

Table 17: Minimal matrix representations of all acute $0/1$-simplices in I^3, I^4 and I^5.

Table 18: Minimal matrix representations of all six acute $0/1$-simplices in I^6.

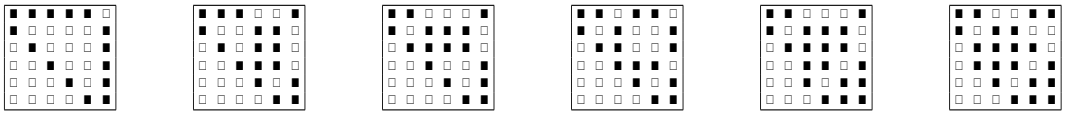

Table 19: Minimal matrix representations of all thirteen acute $0/1$-simplices in I^7.

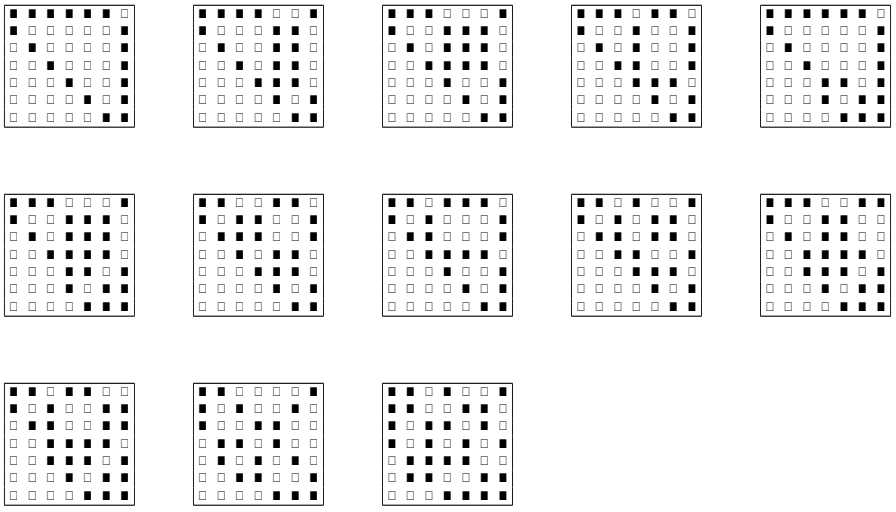

Table 20: Minimal matrix representations of all twenty-nine acute 0/1-8-simplices.

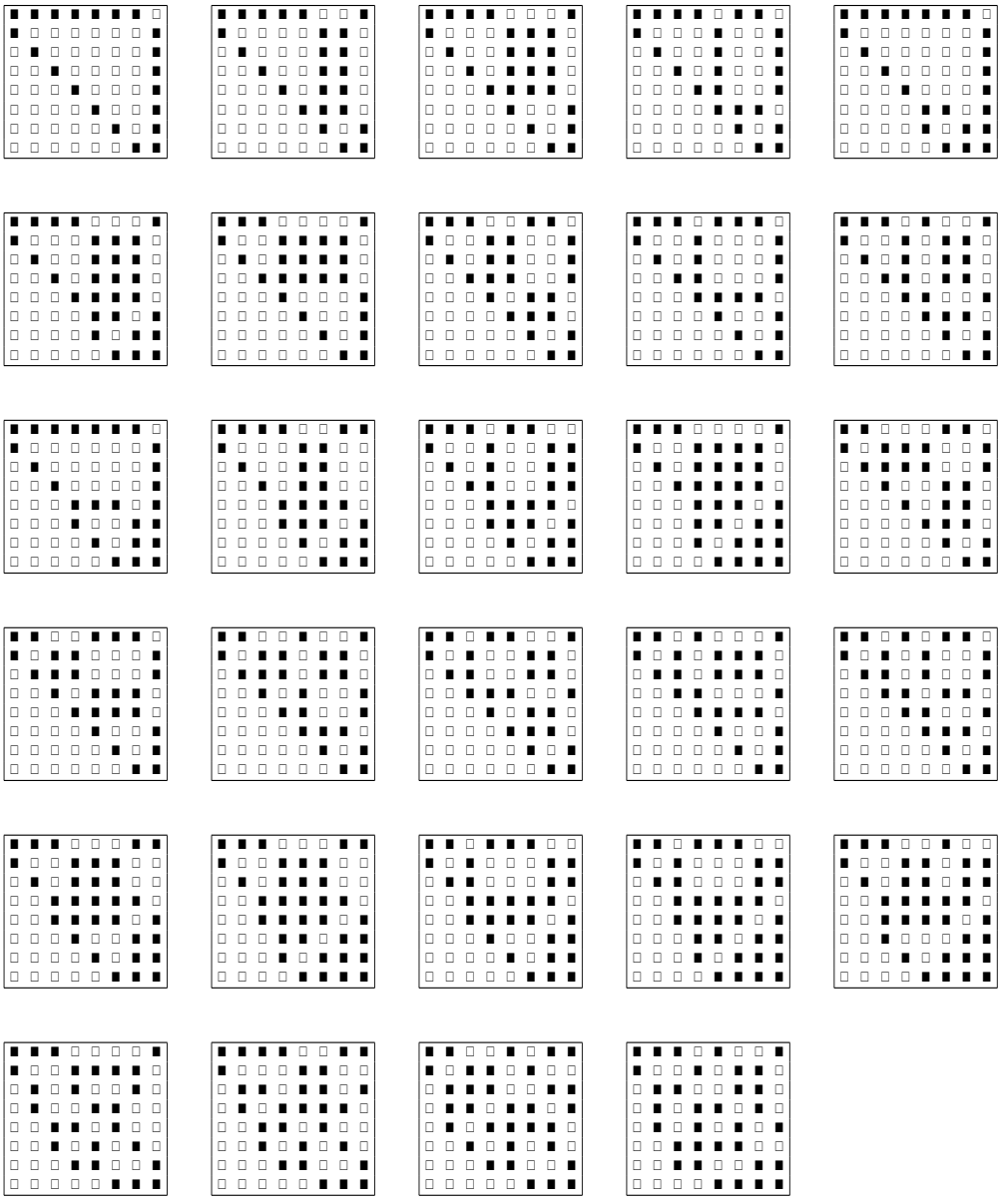

Table 21: Minimal matrix representations of the first 35 acute 0/1-9-simplices.

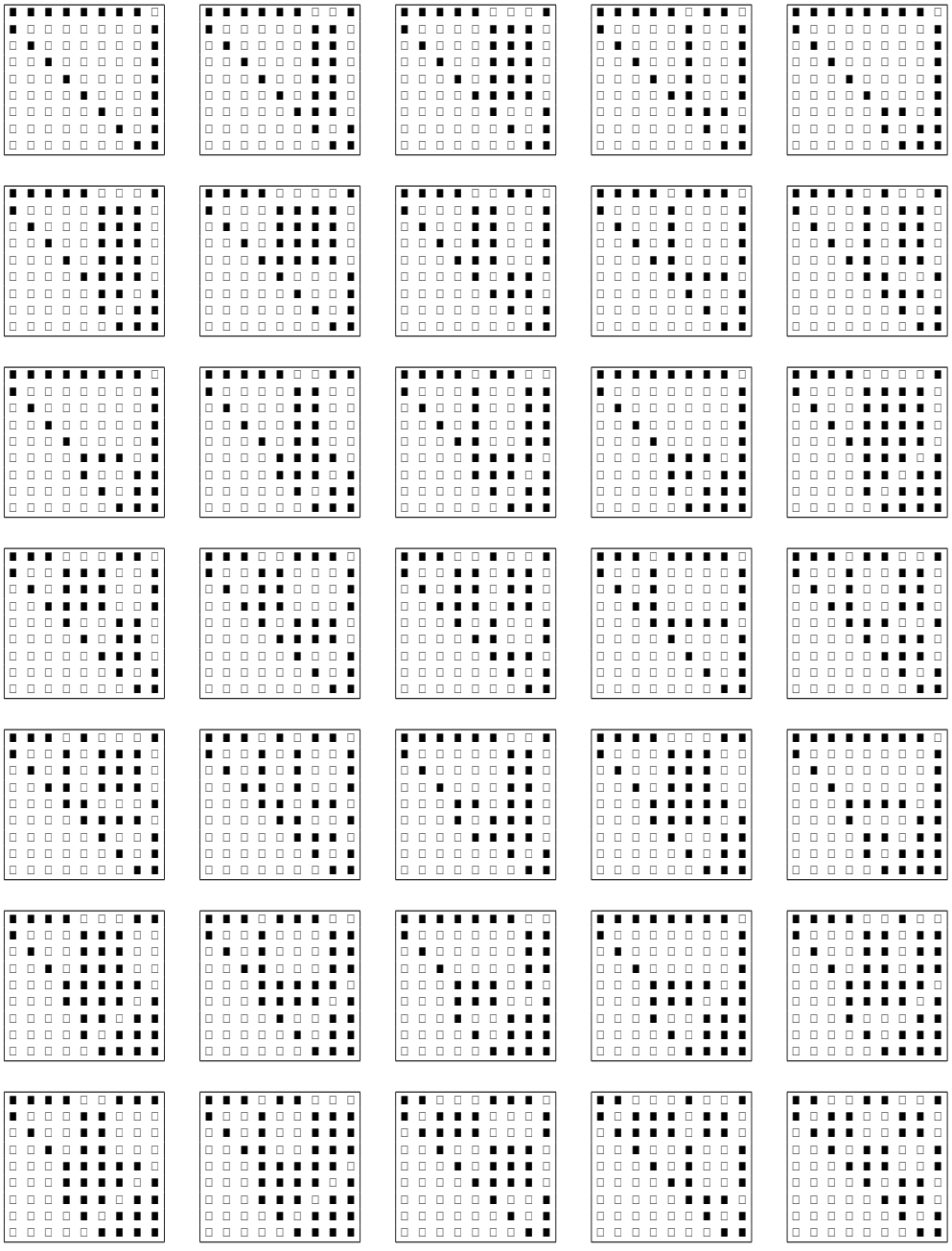

Table 22: Minimal matrix representations of the remaining 32 acute 0/1-9-simplices.

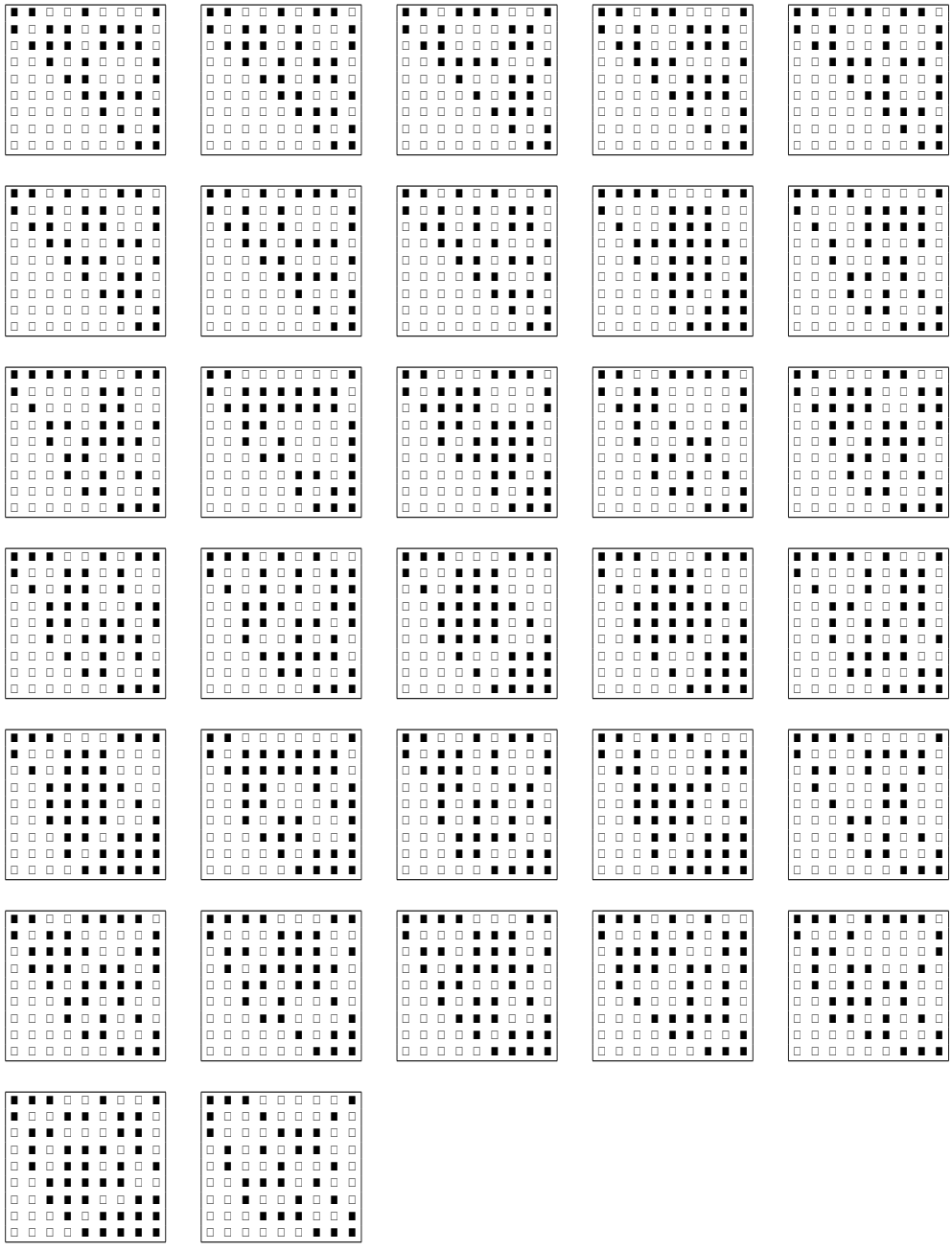

A.3.1 Minimal matrix representations of acute 0/1-3, 4, 5, 6, 7-simplices

There are 1, 1, 2 acute 0/1-simplices in I^3, I^4, I^5 respectively modulo the action of the hyperoctahedral group. The absolute values of the determinants of their minimal matrix representatives given below are in the set

$$\det_3 = \{2\}, \quad \det_4 = \{3\}, \quad \det_5 = \{4, 5\}. \tag{75}$$

There are 6 acute 0/1-simplices in I^6 modulo the action of $\mathcal{B}_6$. The absolute determinants of their minimal matrix representatives given below are in the set

$$\det_6 = \{5, 7, 8, 9\}. \tag{76}$$

In I^7 there are 13 acute 0/1-simplices modulo the action of $\mathcal{B}_7$. The determinants of their minimal matrix representatives given below are in the set

$$\det_7 = \{6, 9, 10, 11, 12, 13, 14, 24, 32\}. \tag{77}$$

A.3.2 Minimal matrix representations of acute 0/1-8-simplices

There are 29 acute 0/1-8-simplices in I^8 modulo the action of $\mathcal{B}_8$. The determinants of their minimal matrix representatives given below are in the set

$$\det_8 = \{7, 11, 13, 14, 15, 16, 17, 18, 19, 20, 21, 22, 23, 40, 44, 56\}. \tag{78}$$

A.3.3 Minimal matrix representations of acute 0/1-9-simplices

There are 67 acute 0/1-9-simplices in I^9 modulo the action of $\mathcal{B}_9$. Their absolute determinants are

$$\det_9 = \{8, 13, 16, 17, 19, 20, 21, 22, 23, 24, 25, 26, 27, 28, 29, 30, 31, 32, 34, 35, 45\}$$

$$\cup\{56, 64, 68, 72, 80, 88, 96\}.$$

References

[1] E.J. Aiton, A.M. Duncan, and J.V. Field (1997). Excerpt from Book III of Harmonices Mundi by Johannes Kepler (1619), translated with an Introduction. *Memoirs of the American Philosophical Society*, 209:163.

[2] J.H. Brandts and A. Cihangir (2013). Counting triangles that share their vertices with the unit n-cube. *Proc. Conf. Applications of Mathematics*, (J.H. Brandts, S. Korotov, M. Křížek, J. Šístek and T. Vejchodský, Eds.) Institute of Mathematics AS CR, Prague, ISBN 978-80-85823-61-5, pp. 1–13.

[3] J.H. Brandts and A. Cihangir (2016). Geometric aspects of the symmetric inverse M-matrix problem. *Linear Alg. Appl.* 506:33-81.

[4] J.H. Brandts, S.Q. Dijkhuis, V. de Haan, and M. Křížek (2013). There are only two nonobtuse triangulations of the unit n-cube. *Computational Geometry, Theory and Applications*, 46(3):286–297.

[5] J.H. Brandts, J. van den Hooff, C. Kuiper, and R. Steenkamp (2012). From binary cube triangulations to acute binary simplices. *Proc. Conf. Applications of Mathematics*, (J.H. Brandts, J. Chleboun, S. Korotov, K. Segeth, J. Šístek, T. Vejchodský (Eds.) Institute of Mathematics AS CR, Prague, ISBN 978-80-85823-60-8, pp. 31–42.

[6] J.H. Brandts, S. Korotov, and M. Křížek (2007). Dissection of the path-simplex in $\mathbb{R}^n$ into n path-subsimplices. *Linear Alg. Appl.* 21(2-3):382–393.

[7] J.H. Brandts, S. Korotov, M. Křížek, and J. Šolc (2009). On acute and nonobtuse simplicial partitions. *SIAM Rev* 51(2):317–335.

[8] R.A. Brualdi (2010). *Introductory Combinatorics* (5th ed.), Chapter 14: Pólya Counting. Upper Saddle River, NJ: Prentice Hall, pp. 541-575

[9] R.A. Brualdi and H.J. Ryser (1991). *Combinatorical Matrix Theory*. Cambridge University Press, Cambridge.
[10] W.Y.C. Chen (1993). Induced cycle structures of the hyperoctahedral group. *SIAM J. Discrete Math.*, 6(3)353–362.
[11] W.Y.C. Chen and P.L. Guo (2014). Equivalence classes of full-dimensional 0/1-polytopes with many vertices. *Discrete Comput. Geom.* 52(2):630–662.
[12] L. Ching (1993). The maximum determinant of an $n \times n$ lower Hessenberg $(0, l)$ matrix. *Linear Algebra Appl.*, 183:147–153.
[13] A. Cihangir (2015). On 0/1-polytopes with nonobtuse triangulations. *Appl. Math. Computation*, 267(C):17–27.
[14] C. Dellacherie, S. Martinez, and J. San Martin (2014). *Inverse M-matrices and ultrametric matrices*. Springer Lecture Notes in Maths 2118.
[15] G. Ehrlich (1973) Loopless algorithms for generating permutations, combinations, and other combinatorial configurations, ACM, 20:500513.
[16] M. Fiedler (1957). Über qualitative Winkeleigenschaften der Simplexe. *Czechoslovak Math. J.* 7(82):463–478.
[17] L. Geissinger and D. Kinch (1978). Representations of the hyperoctahedral groups, *J. Algebra*, 53:1–20.
[18] N.A. Grigoriev (1982). Regular simplices inscribed in a cube and Hadamard Matrices. *Proceedings of the Steklov Institute of Mathematics*, 152:97–98.
[19] J. Hadamard (1893). Résolution d'une question relative aux déterminants. *Bull. des Sciences Math.* 2:240-246.
[20] M. A. Harrison and R.G. High (1968). On the cycle index of a product of permutation groups, *J. Combin. Theory*, 4:277–299.
[21] C.R. Johnson (1982) *Inverse M-matrices. Linear Algebra Appl.*, 47:195–216.
[22] C.R. Johnson and R.L. Smith (2011). Inverse M-matrices, II. *Linear Algebra Appl.*, 435:953–983.
[23] G. Kalai and G.M. Ziegler (Eds) (2000). *Polytopes - Combinatorics and Computation*. DMV Seminar, Band 29, Birkhäuser Verlag, Basel, Boston, Berlin.
[24] C. Kimberling and P.J.V. Moses (2014). The infinite Fibonacci tree and other trees generated by rules. *Fibonacci Quart.*, 52(5):136–149.
[25] D.E. Knuth (2009). *The Art of Computer Programming Vol. 4, Combinatorial Algorithms, Fasc. 3b, Generating all partitions*. Pearson Education (US).
[26] R. Nabben and R. Varga (1994). A linear algebra proof that the inverse of a strictly ultrametric matrix is a strictly diagonally dominant Stieltjes matrix. *SIAM J. Matrix Anal. Appl.*, 15(1):107–113.
[27] G. Pólya (1937). Kombinatorische Anzahlbestimmungen für Gruppen, Graphen, und chemische Verbindungen, *Acta Math.*, 68:145–253.
[28] C. Zong (2005). What is known about unit cubes? *Bulletin (New Series) of the AMS*, 42(2):181–211.
[29] The On-line Encyclopedia of Integer Sequences (1964). Founded by N.J.A. Sloane. http://oeis.org